A Tool for Probabilistic Evaluation of Microgrid Operating Strategies with Demand Side Management

Submitted in partial fulfillment of the requirements for

the degree of

Doctor of Philosophy

in

Electrical and Computer Engineering

Jesse A. Thornburg

S.B., Mechanical Engineering, Massachusetts Institute of Technology
S.B., Comparative Media Studies, Massachusetts Institute of Technology
M.S., Electrical and Computer Engineering, Carnegie Mellon University

Carnegie Mellon University
Pittsburgh, PA

December 2018

The more you lose yourself in something bigger than yourself, the more energy you will have.

- Norman Vincent Peale

Dedicated to my parents, Gene and Shannon Thornburg,

and to Megan Moffett

Abstract

Smart meters in microgrids enable fine-grained monitoring and control of individual building demands. Possibilities are being explored globally to leverage these smart meter capabilities for demand side management (DSM), particularly to advance rural electrification in emerging contexts. Simulating different microgrid configurations and operating strategies before implementing them is valuable for providing reliable service to customers and keeping expenses low. This dissertation focuses on the design, development, and implementation of a simulation tool that quantitatively compares microgrid operating strategies and sizing options. To this end, the tool's pre-processing engine accepts arbitrary parameters for probability distributions to characterize loads and nondispatchable supplies (e.g., wind and PV). This dissertation presents methods to compute probability distributions for the aggregate system demand from individual load distributions that characterize each consumer. Further computational methods are given to derive probabilistic estimates of aggregate loads reduced by DSM. These probability underpinnings create effective system-level models for simulation studies of energy management schemes. The models of aggregate load behavior and probabilistic supply are used in a simulation model that includes dispatchable generation and storage components to perform Monte Carlo simulation studies.

This dissertation describes the rationale and modeling parameters for different components in the simulation tool. The tool allows different rule-based energy management strategies to be implemented and compared, with certain supplies and storage options being controllable while others are driven by external factors. To account for the wide range of possible outcomes that occur in a real-world system, the tool is fundamentally probabilistic and runs its MATLAB/Simulink-based microgrid model with Monte Carlo methods. The loads can be designated Markovian or independent-in-time. The Energy Manager makes dispatch decisions with limited knowledge of the rest of the system, similar to controllers in real-world microgrids. The Energy Manager also limits certain loads with DSM to meet system goals, e.g., to reduce the incidence of power cuts or limit fuel-burning generation. The Energy Manager can prioritize renewable generation, energy storage, etc. as desired by the microgrid operators. To demonstrate the simulation tool, this dissertation concludes with case studies based on a microgrid in

Rwanda. The case studies provide examples of how smart meters, which are able to control residential demand, can benefit microgrid operations. The deployment of DSM strategies using smart meters is shown to reduce the occurrence and duration of power cuts when system demand exceeds the total available supply.

Acknowledgments

This dissertation could not have been completed without the support of a host of advisors, friends, and family. Thank you to Bruce Krogh for advising me throughout the program and serving as doctoral committee chair. Thanks to Gabriela Hug and Taha Selim Ustun for their helpful advising at different stints of the program. Many thanks to Bruce, Gabriela, M. Granger Morgan, and Anthony Rowe for serving on my doctoral committee. I also gratefully acknowledge this was made possible by grants from NSF GRFP (Grant No. DGE-1252522) and the DOE-funded Hydropower Foundation. With the Hydropower Foundation Norm Bishop, Brenna Vaughn, Bree Mendlin, and Deborah Linke have supported me as mentors and friends in addition to providing needed funding.

Encouragement and guidance have come from the members of Gabriela's research group who helped me acclimate to PhD research and life in Pittsburgh. This supportive group includes Javad Mohammadi, Xiao Zhang, Junyao Guo, Andrew Hamann, and Dmitry Shchetinin. Special thanks to Javad and Hadi Amini for long days collaborating on ways to commercialize and scale parts of our research. Thanks to Claire Bauerle for her assistance handling reimbursements, room bookings, video conference setup, etc. as advisors (and sometimes myself) were overseas.

Thanks to Nathan Williams and Chukwudi Udeani of the Engineering and Public Policy (EPP) department for joining me in founding the Infrastructure Systems for Global Development (ISGD) group and collaborating there. Helpful discussions with Rebecca Ciez, Matthew Babcock, Brian Sergi, Aviva Loew, and Nathan provided insights on energy policy, financing, and funding. Publishing with each of them stretched me and pushed me to consider public policy ramifications in my work.

Finally, I want to thank my family and supportive friends outside CMU for their moral support and listening ears. My parents Gene and Shannon instilled the work ethic and outlook that brought me to this program and through it. My siblings Luke, Whitney, Josh, and Hannah helped me keep work in perspective and not take things too seriously. To Megan Moffett, thank you for listening and talking with me through so many frustrating periods of this work, from across the world and together in Pittsburgh. You've brightened the dead ends and times of searching, and the best is yet to come.

Contents

Acronyms

AGC automatic generation control. 35, 38, 58

CFL compact fluorescent light. 51

DSM demand side management. 1, 2, 4, 7–9, 17, 26, 30, 37, 58, 60, 62, 65, 69, 70, 72

EM energy manager. 12, 20, 27–29, 31, 32, 34–40, 42, 43, 50, 55, 58, 65, 71–73

EV electric vehicle. 8

FFT fast Fourier transform. 20

HOMER Hybrid Optimization Model for Electric Renewables. 10–12

HVAC heating, ventilation, and air conditioning. 8

LOLP loss of load probability. 12

O & M operations and maintenance. 34

OECD the Organisation for Economic Co-operation and Development. 8

PLASMiS Probabilistic Load-Attenuating Smart Microgrid Simulator. xii, 3–5, 12–15, 17, 18, 20, 27–40, 44, 48, 49, 52, 55, 57, 58, 69–73

PMF probability mass function. 13–15, 17–19, 21, 28, 32, 33, 39, 45, 69

PV photovoltaics. 3, 9, 33, 34, 48, 49, 51–53, 55, 59, 62

RV random variable. 13–22, 26, 28, 32, 69

SME smart-meter-enabled. 1, 4, 6–9, 70

SOC state of charge. 36, 37, 42, 53, 72

STEMM Stochastic Techno-Economic Microgrid Model. 11, 12

List of Tables

List of Figures

Chapter 1

Introduction

The US Department of Energy (DOE) defines a microgrid as "an integrated energy system consisting of interconnected loads and distributed energy resources." DOE adds that coordination is key and the term microgrid does not apply to "a group of individual generation sources that are not coordinated" [55]. The International Council on Large Electric Systems (CIGRE) further clarifies that the term microgrid applies exclusively to such an energy system on a distribution network (no high voltage or transmission lines), i.e., a single bus power system [10]. A microgrid is called islanded when it has no connection to a utility grid (no infinite bus in the system) and a lack of grid services like operating reserves. Challenges arise in islanded microgrids when the installed generation has insufficient capacity to meet growing demand and when this generation is increasingly supplied by intermittent renewable sources. The integration of smart meters into islanded microgrids brings the system managers new operational flexibility and monitoring capabilities. Specifically, smart meters with load management functionality allow demand side management (DSM) at fine time granularities and on a load-by-load basis [18]. This dissertation focuses on modeling and simulation of smart-meter-enabled (SME) islanded microgrids with DSM capabilities.

Load management is a valuable feature for microgrids, which typically lack some dispatchable features of transmission networks like spinning reserves and grid-scale storage (e.g., pumped hydropower reservoirs). With these limitations, SME microgrids can employ dispatch strategies that are often time-dependent and combine control of loads and supplies. In addition, the grow-

ing availability of lead acid batteries in rural developing contexts makes storage charging and discharging an important consideration in dispatch strategies [28]. On the demand side, load management is increasingly flexible with smart meters capable of load attenuation, i.e., reducing individual loads to a power limit (or cutting certain loads entirely) to avoid a full system power cut or localized brownout [18]. This method of limiting loads, attenuating individual loads to fixed power limits without cutting any load entirely, will be termed *clipping* in this dissertation. As microgrids are becoming equipped with smart meters capable of clipping, flexible DSM techniques that use clipping can be tested and evaluated in simulation [61], [59], [60], [58]. Simulation tools that incorporate these new operational choices are valuable for smart microgrid planning and operations, allowing investors and microgrid managers to anticipate the options for load management to choose and operate energy assets accordingly.

In recent years microgrid managers have begun clipping for load management in select microgrids of Haiti, Nigeria, Tanzania, and Bhutan [18], [51]. Microgrids consist of significantly different architectures and equipment mixes depending on a region's infrastructure and level of development. Microgrids in the developing world constitute a special case, where customer demand is unpredictable and often grows rapidly when electricity becomes available for the first time. These microgrids often suffer from insufficient supply when customer loads exceed the levels anticipated during microgrid planning [18]. Islanded microgrids that run independently of any larger grid are a staple for electricity distribution in the developing world. They prove especially important in rural areas where utility grids are limited in their coverage or reliability.

Expanding electricity access provides many economic and developmental benefits. Average income, quality of life, health, and access to information all increase when a community first receives access to electricity [76]. As this access becomes a higher priority in the developing world, distributed energy systems are necessary where utility grids are limited or absent altogether [69]. Many developing countries have little capital allocated to utility grid infrastructure, and these countries often lack any private firm equipped to provide widespread energy access [54]. For these reasons, microgrids are a desirable solution for expanding energy access. In Rwanda, for example, the national utility Rwanda Energy Group (REG) anticipates 48% of the population will receive power from microgrids indefinitely, with no plan to connect these (typically rural) homes to the national grid [25]. With microgrids proliferating and smart meters becoming more afford-

able, the process of incorporating smart meters into microgrid operations is rapidly spreading across the developing world. For energy development in these countries, a tool that models smart meter capabilities is necessary for efficiency in microgrid planning and management. Given the high variability of instantaneous demand and available supply in developing world microgrids, a tool that models more than anticipated cases (or an average/expected case) would be helpful, specifically a tool that models the full range of possible situations stochastically. In general, an effective simulation tool for microgrids must model the physical elements in sufficient detail to obtain useful results but keep these models simple enough to produce system-level metrics efficiently.

This dissertation presents a simulation tool called the Probabilistic Load-Attenuating Smart Microgrid Simulator (PLASMiS). PLASMiS models and evaluates microgrid operating strategies for different generator and load types, integrating dispatchable and nondispatchable[1] supplies with energy storage and various types of loads (controllable and uncontrollable). Among the supply options modelled in PLASMiS are renewable sources, specifically photovoltaics (PV) and wind. These are modeled as nondispatchable with probabilistic natural resource inputs. Renewables can also be modeled in PLASMiS as dispatchable with time-dependent limits on their outputs. PLASMiS is especially designed to simulate and compare microgrid operationing strategies, e.g., dispatch strategies for battery storage and smart meter load management. Testing across this breadth of inputs, PLASMiS is also useful for microgrid planning and the cost-effective implementation of smart meters. With stochastic models defining loads and nondispatchable supplies, PLASMiS uses Monte Carlo simulation to probabilistically characterize the full range of possible supply and demand profiles.

This dissertation makes contributions by developing:

- A formula for computing aggregate Markov transition matrices to characterize the sum of independent Markovian random variables (RVs), with derivation (Chapter 3, Sections 3.3 to 3.4).

- Computational methods for bounding the value of aggregate clipped load, given aggregate unclipped load (Chapter 3, Section 3.5)

[1]Nondispatchable supplies are driven by external factors (e.g., solar irradiance or wind velocity) that are modeled as stochastic. Thus nondispatchable generation is left uncontrolled by PLASMiS.

- A rationale for modeling generation and storage dispatch with load clipping as a DSM technique (Chapter 4)
- PLASMiS, a probabilistic simulator for microgrids for evaluating microgrid operations and planning by quantitative metrics (Chapter 5)
- A rationale for sizing generation in case studies as a first pass for microgrid planning (Chapter 6, Sections 6.2 and 6.6)
- Case studies modeled after rural microgrids in Rwanda, tested in PLASMiS (Chapter 6, Sections 6.3 to 6.4)
- Case study results demonstrating the effects of changing clipped load power limits and the number of clipped loads, both demonstrated with the Rwanda microgrid model (Chapter 7)
- A quantitative justification for the intelligent use of load clipping to mitigate power cuts in islanded microgrid operations. (Chapter 7)

These contributions fall into several major categories. The first two are mathematical derivations for reducing computational complexity and forecasting given a state change, respectively. The remainder of the contributions detail a probabilistic model for simulating islanded, SME microgrids and the introduction of a new tool (PLASMiS) to perform these simulations with different DSM and operating strategies.

The following chapters describe the context and motivation for this work, the simulator rationale and design, and different uses for PLASMiS demonstrated in the aforementioned case studies. Chapter 2 shares background, including an overview of prior microgrid simulation tools and their differences from PLASMiS. Chapter 3 explains the mathematical derivations of probabilistic models used for microgrid simulations over the full range of their supply and demand scenarios. Chapter 4 gives the modeling approach for real-world microgrid components simulated in PLASMiS, with discussion of rule-based energy management. Chapter 5 shows the design rationale and structure of PLASMiS from pre-processing to Monte Carlo simulation to post-processing. Section 6 explains the design of case studies to demonstrate certain capabilities

of PLASMiS. Chapter 7 describes the tests performed and results of these case studies. Finally, Chapter 8 presents conclusions including directions for future work that can be carried out to extend the capabilities and applications of PLASMiS.

Chapter 2

Background and Related Work

2.1 Introduction

Microgrids are growing in popularity around the globe. They serve as research topics for the academic community, as investment opportunities in the power industry, and as sources of energy security for consumers themselves. Smart meters provide a fertile area for microgrid research, since they can enable real-time load control while also producing data at high granularity for aggregation and analysis [58],[61],[59]. Prior research on SME microgrids includes recent field implementations and a range of deterministic models and simulators [18],[51]. In this chapter, a summary of popular microgrid simulation tools reveals significant modeling support that addresses microgrid planning and sizing. Studies performed with the existing tools demonstrate many options made possible with smart meters, including quantitative microgrid planning and economic analyses. Simulating operational strategies is less often supported with widely available simulators.

2.2 Smart Meters in Microgrids

Smart meters deployed in microgrids are starting to enable real-time load aggregation measurements as well as fine-grained monitoring and control, including load clipping to prevent power cuts [60],[18],[58]. This new functionality makes it possible to envision and implement new operating strategies for microgrid managers [59],[60],[61]. Load clipping reduces instantaneous

demand to prevent power cuts when system demand exceeds supply. By using smart meters, dispatchable supplies can be controlled and demand limited to avoid power cuts [36], [72]. The demand-side smart meters referenced in this dissertation are of the type currently deployed across Africa, Latin America, and India, which range in price from $9 to $87 [56]. The units available for developing contexts can be for AC or DC systems [13], [2], and they are designed to run for 10-15 years [78]. Taking the SparkMeter as a prime example, the smart meters modeled in this dissertation are equipped to limit demanded power to a clipped power limit [53]. This limit is specified by a central gateway controller that maintains wireless two-way communication with all smart meters in the microgrid while storing their data to the cloud [44]. Load clipping is a type of DSM enabled by certain smart meters, including the SparkMeter, that have been introduced in the field around 2010 [18], [51]. Microgrids instrumented with these smart meters need not rely on traditional hard-coded, binary control from simple current limiters. On the economic side, electricity pricing can be tied to clipping limit, incentivizing customers to accept clipping since doing that gives them a discount on power. Customers choosing lower clipping limits gives the microgrid manager more flexibility to smooth or flatten the load curve in peak hours and thus reduce the likelihood of a power cut. Dispatch schemes that dynamically dispatch generation and energy storage can be paired with load clipping to further decrease the incidence of power cuts [66]. Broad categories of supply, storage, and demand inputs an SME microgrid with these capabilities is shown in Fig. 2.1, and Chapter 4 gives further details on each labeled item.

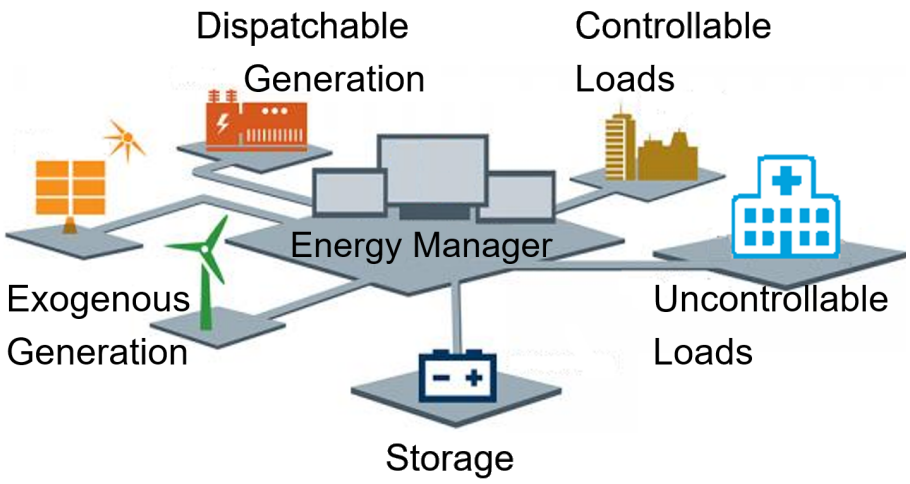

Figure 2.1: Schematic diagram of an SME microgrid with clipping DSM [77]

In practice, smart meters are increasingly being installed in the Organisation for Economic Co-operation and Development (OECD) nations as well as developing countries. Major electronics and controls companies such as Eaton, Siemens, and Schneider Electric are selling smart meters together with microgrid controllers as they propogate SME microgrids in Western nations [77]. This dissertation focuses instead on microgrids in developing countries. In these contexts, microgrids are proliferating as the demand for smart meters grows year over year [12], with notable increases especially across Africa and the Middle East [78]. Africa specifically sees rapid adoption of the technology, given the lack of legacy infrastructure or expectation from the general public of a centrally managed power system (i.e., a utility grid). Given these two factors rural communities in Africa are skipping traditional energy technologies which, once in place, have kept more developed nations from adopting the latest infrastructure technologies including smart meters [78]. Load clipping is essential for preventing power cuts in these microgrids where demand growth that is often unpredictable strains microgrid systems with undersized generation and limited capital for new generation [18], [43].

2.3 DSM Techniques

Relevant work on microgrid operations focuses on DSM options with charging and discharging of storage elements. Much of the previous DSM research focuses on load shifting, especially with heating, ventilation, and air conditioning (HVAC) and electric vehicle (EV) loads. Wei et al. model EV charging as a time-shiftable load and control the power delivered to each EV battery for a given time interval [71]. Niinisto describes a load shifting algorithm that smooths forecast error from aggregated demand and weather-dependent generators [48]. As with dynamic load shifting, scheduling loads beforehand must follow constraints to meet consumer needs (e.g., not scheduling appliances to run at a future time when they are no longer useful) [71]. Temporarily cutting certain loads entirely is another DSM technique. Grids have historically been able to cut individual loads, either when a given load exceeds a current or power limit (e.g., with breakers and fuses) or when a customer's credit for electricity runs out (e.g., with a prepaid electricity meter) [57]. The research presented in this dissertation considers the contributions of smart meters in dynamically clipping loads, a DSM method that is new to the modeling landscape.

Load clipping in SME microgrids has been implemented in several incarnations throughout the developing world. The GridShares program in Bhutan installed smart meters in 90 homes and runs them with clipping automatically applied when microgrid voltage falls below a threshold value. Clipping in their implementation is prescribed and rigid, performed equally across all customers with the voltage threshold enforced at all times [51]. More variation in clipping options are introduced by SparkMeter through their instrumented microgrids in Haiti and Tanzania. Their smart meters apply different peak power limits to different customers based on the electricity tariff chosen by the customer. Higher tariffs correspond with higher peak power limits. Customers pre-pay for electricity at a tariff level corresponding to the clipping limit they choose. The microgrid manager can actuate the meters together or each meter separately as needed, e.g., to cut off service to a business that has stopped paying for electricity [18]. This dissertation work assumes load-clipping functionality in the smart meters modeled here, focusing on SME microgrids like that of SparkMeter, where loads can be constrained to peak power limits of arbitrary magnitude. GridShares and SparkMeter have each demonstrated viable smart meters for clipping, and they have verified load clipping in the field with these devices.

2.4 Simulation Tools for Microgrids

Planning for DSM, supply sizing, and microgrid operations enables less onsite engineering and troubleshooting, which reduces costs for installation and maintenance. Certain planning tasks for grid development, e.g., sizing of PV, have been the focus of research using computational optimization methods without the need for a dedicated simulation tool [49],[39]. These approaches typically optimize for a specific context or goal, e.g., maximum power generated from solar energy over a typical day based on conditions at a selected site [65],[40]. Optimizing the topology of an electrical network is similarly a research topic often addressed algorithmically (e.g., with machine learning) [21]. Microgrid testbeds provide a physical platform for testing [66], but these require much higher upfront capital than a software-based simulation tool. A simulation tool can model microgrids of different designs with arbitrary user-defined inputs, offering greater flexibility than a testbed, computational exercise, or purely algorithmic approach.

Testing microgrid strategies and designs in simulated case studies before implementing them

in practice can save microgrid developers significant time and money. Developers therefore choose simulation tools to reduce risk and improve rates of return [19]. Approaches to optimally plan and model transmission networks (topology, phase balance, and power flow) have been in use for over a century [26], while dynamic, quantitative modeling of distribution-level microgrids is a much more recent development. Current simulators often focus on microgrid planning, as designers and project managers aim to minimize the large capital outlay required for building and maintaining a microgrid [9]. Three popular tools that address planning concerns are described below. Two other topics less frequently addressed by microgrid simulators are daily operations and dispatch. These prove important from a business perspective given the economic imperative to fund a microgrid day-to-day through generated income. The most popular microgrid simulation tools available today do not allow offline assessment and evaluation of supply dispatch and load clipping strategies, which leaves microgrid operators relying on broad rules of thumb, real-time experimentation, and intuition when implementing load clipping.

One factor that has limited the scope of microgrid simulation is the preponderance of deterministic simulators and those focused on transmission-level systems [14]. To address inherent variation in supply and demand levels, probabilistic modeling and dynamic control options are needed to prevent power imbalance in the microgrid system. Three tools that are currently available, both deterministic and probabilistic, are described below.

The Hybrid Optimization Model for Electric Renewables (HOMER) is a popular simulator for microgrid planning, specifically for sizing of generation and storage. HOMER models real power and chooses the optimal sizes and generation types to supply given microgrid loads and meet other objectives (e.g., maximum income, minimal emissions, etc.) [50], [17]. HOMER is fundamentally deterministic but can perform boundary analysis (evaluating max/min cases) with variability parameters input by the user [74]. HOMER runs with one-hour time increments. Regarding dispatch strategies, HOMER performs simulations in two preset dispatch strategies and compares the two. These fixed strategies are cycle charging, where the generators are deployed to charge the battery storage, and load following, where the generators provide just enough power to meet load without battery charging [9]. HOMER's optimization criteria are focused on maximum net income, with consideration of depreciation and life cycle costs. HOMER allows for DSM by accepting schedules for certain time-flexible loads. The user can also designate primary

loads (that must be met on a certain schedule), deferrable loads (loads that can be met flexibly within a given time span), and thermal loads (demand for heat, e.g., with CCGT generation) [37].

GridLAB-D is a popular simulator for power network design, specifically planning distribution systems. GridLAB-D models reactive as well as real power. It integrates coupled differential equations and can operate with time steps of less than one second [63]. GridLAB-D is deterministic and does not have the capacity for probabilistic analysis. In terms of dispatch, GridLAB-D performs standard economic dispatch and includes models of power electronics components (e.g., inverters and variable capacitive loads). GridLAB-D incorporates a wholesale market model and price-responsive appliance controls (sending setpoints based on the market electricity price) to reduce peak demand or maximize microgrid income. GridLAB-D models reactive power control by managing certain capacitive and inductive loads in the system according to the needs of the distribution network. For example, GridLAB-D performs Volt/VAR control to switch capacitive elements on and off in order to maintain a desired voltage [8].

The Stochastic Techno-Economic Microgrid Model (STEMM) is a microgrid and electricity market simulator for economic planning and generation sizing. STEMM is built using the general-purpose quantitative modeling tool Analytica [73]. STEMM models real power and characterizes loads and nondispatchable supplies from user-specified parameters for certain distributions. STEMM employs Monte Carlo methods for probabilistic analyses, which it applies to optimal generation planning to maximize economic returns. For example, STEMM was recently used to optimally size new PV arrays for maximum net income in a microgrid with diesel generation and battery storage [75]. In its advanced economic model STEMM also accounts for nontechnical losses due to operational inefficiencies, power theft, and non-payment [73]. STEMM can take parameters for a set of probability distributions as inputs to characterize uncertain load inputs. The storage subsystem models a lead acid battery bank. STEMM focuses on maximizing economic returns, accounting for expenses funded by income dependent on electricity pricing. STEMM tracks the net present value of capital equipment and the price elasticity of demand. The tool employs load scheduling DSM, similar to HOMER [73]. In its discrete timeline, STEMM has a one-hour time step like HOMER [75].

STEMM is well suited to microgrid planning and supply sizing, with its Monte Carlo analysis ideal to assess the full range of operating conditions and choose a microgrid's generation

accordingly [73]. At present, STEMM is internal to Carnegie Mellon University, where it was developed in the Department of Engineering and Public Policy. The software is currently being re-coded in Python for a web-based platform, to be released publicly by the end of 2019.

These popular simulators have many similarities. STEMM, HOMER, and GridLAB-D all feature dispatchable battery storage in hybrid microgrids with renewable and fossil-burning generators [8], [59], [73], [68]. All three simulators model controllable generation as dispatchable and perform economic dispatch at each time step. STEMM, HOMER, and GridLAB-D model dispatching generation and managing storage using an implicit controller that assumes sufficient knowledge of the system at all times. They do not have an explicit model of the power system "plant" providing signals to a separate controller, which could have limited knowledge. PLASMiS, on the other hand, has a realistic signal flow model and explicit energy manager (EM) model. In this approach the EM with limited knowledge forecasts load and nondispatchable supply which are fully known in its distribution network model. The EM thus can be configured to work with imperfect or noisy information to provide the network with dispatch commands. Like STEMM, PLASMiS accounts for generation losses due to machine inefficiencies [73]. In contrast to STEMM, PLASMiS is best equipped to compare and evaluate different operating strategies, with given generator types and sizing fixed [61], [59].

PLASMiS runs in discrete time like HOMER and STEMM. PLASMiS, however, runs with a basic one-minute time step, a much finer granularity than the one-hour time step of HOMER and STEMM. Flexibility in sample times is built into the PLASMiS EM, which sends setpoints and state commands to the plant at a constant EM sample time, an arbitrary number of minutes (a positive integer, i.e., greater than or equal to the time step used in the plant). In the dissertation case studies the EM makes dispatch decisions every 10 minutes (the EM sample time), with supply and demand in the plant model changing every minute (the plant sample time) [61], [59]. Regarding microgrid economics, PLASMiS can compute gross income from electricity tariffs charged over time, but the tool is more focused on dynamic energy management to reduce a microgrid's loss of load probability (LOLP). PLASMiS employs load clipping to prevent power cuts and increase energy sold.

In contrast to the three established tools, PLASMiS is a probabilistic simulator for testing and comparing operating strategies. HOMER and GridLAB-D, as well as some of the most common

transmission network simulators (e.g., PowerWorld [14]), are deterministic and use load and supply curves that are entirely specified [47]. Thus these simulators do not address the path-dependent nature of individual loads [14]. PLASMiS differs from other tools by characterizing loads and nondispatchable supplies stochastically using arbitrary, discrete probability distributions that can be both time-dependent and characterized by Markov models. PLASMiS combines these input distributions through matrix operations into aggregate distributions, which reduces computational complexity [75], [73], [58], [61], [59].

2.5 Probability Background

PLASMiS models each probabilistic quantity (e.g., a load) at a given time as a random variable (RV). An RV is a real-valued function of the outcome of an experiment. In this dissertation, the RVs for different probabilistic quantities are independent with a probability mass function (PMF) for each time step. A PMF is the discretized form of a probability distribution. In PLASMiS, PMFs are used rather than continuous probability distributions to characterize probabilistic quantities that take certain discrete values with specified likelihoods [27].

Individual demands are characterized in PLASMiS as probabilistic quantities, as are natural resources (e.g., solar irradiance and wind velocity). These probabilistic quantities are modeled as random processes (time-sequenced RVs) sampled from time-of-day-dependent PMFs over ranges of integers corresponding to discretizations of the value-space for the quantities. Each probabilistic quantity is modeled by an RV that is either independent in time (no dependence on the value for a given time step on any other time step) or a Markov model (dependent on that quantity's value in the prior time step).

This dissertation denotes time steps by k, $k+1$. Instances of the same quantity (e.g., load) at different time steps are denoted by an index l. With a slight abuse of notation, both an RV and its value will be referred to by the same lower case letter, e.g., x_k^l. Whether an RV or its value is meant in a given instance will be evident from the context.

Each RV in PLASMiS is sampled as index values corresponding to probabilistic quantities (load power, solar irradiance for PV, wind speed for wind turbines, etc.). In PLASMiS all load PMFs and Markov transition matrices (to be discussed below) have rows and columns discretized

to demand levels at a granularity of ϵ, a positive power increment (e.g., in Watts) that is uniform across all RVs that are aggregated together. Since the first entry in each PMF vector (length M^l) corresponds to the zero case, ϵ maps the sampled index i to the power level of $(i-1)\epsilon$ Watts. Similarly, stochastic supply resources like solar irradiance and wind speed each have a constant resource increment (e.g., ζ m/s for wind speed). The output value corresponding to an index i corresponds to resource level $(i-1)\zeta$ m/s. These resource levels and load power values are then fed into the generator models discussed in Chapter 4.

Each RV x_k^l that is independent in time has a PMF $P_k^{x^l}$. The PMF for quantity l is a column vector of length M^l with entries

$$P_k^{x^l}[i] = Pr\{x_k^l = i\}, i \in [1 : M^l] \tag{2.1}$$

In PLASMiS all probabilistic quantities (e.g., loads and nondispatchable supplies) are independent from each other, i.e., the joint probabilites of two such probabilistic inputs (represented by RVs indexed l and m) are

$$Pr\{x_k^l = i, x_k^m = j\} = Pr\{x_k^l = i\}Pr\{x_k^m = j\} \tag{2.2}$$

This independence does not hold for RVs of different time steps for a given probabilistic quantity if that quantity is Markovian.

2.5.1 Markov Models

Markovian RVs by definition have values that are not independent in time but depend on one or more past values. Each Markovian RV modeled in this dissertation is characterized by a discrete-time Markov chain, i.e., the RV sample value for the next time step depends on only the current RV value such that

$$Pr\{x_{k+1}^l = i | x_1^l = a, x_2^l = b, \ldots, x_k^l = j\} = Pr\{x_{k+1}^l = i | x_k^l = j\} \tag{2.3}$$

The conditional PMF is a row vector of length M^l populated with conditional probability values

$$P_{k+1|x_k^l=j}^{x^l}[i] = Pr\{x_{k+1}^l = i | x_k^l = j\} \forall i, j \in [1 : M^l] \tag{2.4}$$

in this case with all possible $k+1$st values conditioned on k^{th} value $x_k^l = i$.

To match a given microgrid's time-based characteristics, in PLASMiS the k to $k+1$ transition probabilities are time-of-day dependent rather than being time-homogenous [70]. Each Markovian RV is characterized by an array of time-of-day-dependent Markov transition matrices $X^l_{k+1|k}$. The $[i,j]^{th}$ element of $X^l_{k+1|k}$ is conditional probability

$$X^l_{k+1|k}[i,j] = Pr\{x^l_{k+1} = j | x^l_k = i\} \tag{2.5}$$

Since the probabilities of an RV transitioning from a given state to each of the other possible states sums to one, each row must sum to one and is a conditional PMF. Thus $X^l_{k+1|k}$ is a right stochastic matrix [24]. $X^l_{k+1|k}$ is a square matrix of size $M^l \times M^l$. To probabilistically determine the value of x^l_{k+1}, $X^l_{k+1|k}$ is narrowed down to one row according to the value of x^l_k. The value x^l_{k+1} is then sampled stochastically from the remaining row.

Whether a given RV x^l_k is independent in time or Markovian, the value of the initial RV, x^l_0, is sampled from PMF $P^{x^l}_0$ (length M^l) rather than from a transition matrix.

2.5.2 Aggregate Probabilistic Quantities

The sum of RVs is itself an RV [27]. A sum of RVs is termed an aggregate RV for the purposes of this dissertation. The aggregate RV for the sum of q independent RVs at time k will be termed

$$a_k = \sum_{l=1}^{q} x^l_k \tag{2.6}$$

where $q \in Z^+$. The PMF characterizing the sum of independent RVs is the convolution of their PMFs [27]. For an aggregate RV a_k representing the sum of $q = 2$ example RVs x^l_k and x^f_k, the aggregate PMF is defined

$$P^a_k = P^{x^l}_k * P^{x^f}_k \tag{2.7}$$

where individual RVs x^l_k and x^f_k are assumed to be recorded in the same increment (discretization of the RVs' value-spaces). For computational benefits this dissertation develops a method for aggregating Markovian RVs and computing an aggregate Markov transition matrix $A_{k+1|k}$, as discussed in Chapter 3.

2.5.3 Monte Carlo Methods

Since the simulation input curves for loads and nondispatchable supplies are generated by random sampling, a high enough number of iterations characterizes a full range of possible outcomes for the dispatch strategy being tested. This testing from repeated random sampling to generate quantitative results is termed a Monte Carlo method, and each run of the simulator is a single Monte Carlo iteration [35].

The simulator inputs RV are sampled for each Monte Carlo iteration. Certain RVs are aggregated before sampling (e.g., small loads like homes) into a single aggregate RV for input to the simulator. Other RVs are sampled individually (e.g., industrial loads, nondispatchable supplies, etc.). When there are many independent instances of a quantity, such as multiple demands from houses, aggregating independent RVs allows computationally efficient sampling and clipping without the need to track the individual RV values, as discussed in Chapter 3.

Chapter 3

Probabilistic Load Models

3.1 Introduction

This chapter presents techniques for modeling individual and aggregate loads in their clipped and unclipped states. To improve performance in PLASMiS, this chapter sets out to compute an aggregate Markov transition matrix $A_{k+1|k}$ of the same form and function as the individual load Markov transition matrix $D^l_{k+1|k}$ but for q summed load RVs. The aggregation process reduces the computational complexity of stochastic sampling (the result of pre-processing in PLASMiS) and running simulations. With the introduction of clipping, a state change complicates load characterization and sampling. This chapter gives mathematical definitions of clipping and computations of clipped aggregate loads that are used to model clipping DSM.

3.2 Notation for RVs

Loads are modeled as Markovian and characterized by transition matrices following the notation in table 3.1. PLASMiS also has the option of modeling loads and nondispatchable supplies as independent in time, i.e., not Markovian and with no path dependency. In the case studies of this dissertation (Chapters 6-7), nondispatchable supplies are modeled as independent in time to demonstrate the independent-in-time option with PLASMiS. Independent-in-time quantities are not modeled with transition matrices but instead with PMFs, computed according to (2.7) for aggregate supplies.

Table 3.1: RVs Used in PLASMiS

Physical Quantities	RV	Type	Increment [Units]
40 Home Loads	d_k^l	Markovian, transition matrix $D_{k+1\|k}^l$	$\epsilon^{d^l}[W]$
Hospital Load	d_k^H	Markovian, transition matrix $D_{k+1\|k}^H$	$\epsilon^{d^H}[W]$
Factory Load	d_k^F	Markovian, transition matrix $D_{k+1\|k}^F$	$\epsilon^{d^F}[W]$
Aggregate Home Load	a_k	Markovian, transition matrix $A_{k+1\|k}$	$\epsilon^{d^l}[W]$
Wind Speed	s_k^w	Nondispatchable Supply - Independent in time	$\zeta[\frac{m}{s}]$
Solar Irradiance	s_k^{PV}	Nondispatchable Supply - Independent in time	$\eta[\frac{W^2}{m}]$

3.3 Computing Aggregate Transition Matrix with Convolution

The aggregate PMF denoted P_k^a characterizes an independent-in-time aggregate load. P_k^a is computed by convolving q individual load PMFs $P_k^{d^l}$ (length M^l for each load l), so P_k^a has length

$$N = 1 - q + \sum_{l=1}^{q} M^l \tag{3.1}$$

P_k^a is computed by iteratively applying (2.7) pairwise until all q individual load PMFs have been convolved. Because a sum of independent RVs is itself an RV (which can then be added to another RV, etc.), the PMF can be computed for the aggregation of an arbitrary number of RVs but represented at each computational step as the sum of two RVs [27]. For the following computations the aggregate of $q \geq 1$ independent RVs will be defined in terms of its final aggregation step, as two individual RVs being summed as follows.

$$a_k = d_k^1 + d_k^2 \tag{3.2}$$

where d_k^2 can represent the previous aggregation of $q - 1$ RVs.

If the individual load RVs x_k^l being aggregated are Markovian, then the aggregate RVs a_k are Markovian. Whether or not the RVs are Markovian, an initial aggregate PMF P_0^a is computed by iteratively applying (2.7) as described above to characterize the initial aggregate RV a_0. For a Markovian aggregate RV, the sample values after time 0 will be determined using time-specific aggregate transition matrices. The aggregate Markov transition matrix $A_{k+1|k}$ will be a square matrix of size $N \times N$ to characterize all possible values of the aggregate load at k and $k+1$. To function like individual transition matrix $D_{k+1|k}^l$ but for aggregate loads, $A_{k+1|k}$ must also be a

right stochastic matrix [24]. The elements of $A_{k+1|k}$ are defined as conditional probabilities

$$A_{k+1|k}[i,j] = Pr\{a_{k+1} = j | a_k = i\} \forall i,j \in [1:N] \tag{3.3}$$

By the definition of conditional probability

$$A_{k+1|k}[i,j] = \frac{Pr\{a_{k+1} = j, a_k = i\}}{Pr\{a_k = i\}} \tag{3.4}$$

The vector of denominator elements $Pr\{a_k = i\}$ is PMF P_k^a computed by (2.7). Therefore each element $P_k^a[i]$ is the constant denominator for the corresponding i^{th} row in $A_{k+1|k}$. The numerator of (3.4) is the $[i,j]^{th}$ element of the joint probability matrix, termed $A_{k+1,k}$ and consisting of the joint probabilities of dependent RVs a_{k+1} and a_k. Expanding the numerator term of (3.4) with the aggregate RV definition in (3.2) gives

$$A_{k+1,k} = Pr\{a_{k+1} = j, a_k = i\} \tag{3.5}$$

$$= \sum_{m=1}^{N} \sum_{n=1}^{N} Pr\{d_{k+1}^1 = n, d_{k+1}^2 = j-n, d_k^1 = m, d_k^2 = i-m\} \tag{3.6}$$

Invoking independence between the two RVs produces

$$A_{k+1,k} = Pr\{a_{k+1} = j, a_k = i\} \tag{3.7}$$

$$= \sum_{m=1}^{N} \sum_{n=1}^{N} Pr\{d_{k+1}^1 = n, d_k^1 = m\} Pr\{d_{k+1}^2 = j-n, d_k^2 = i-m\} \tag{3.8}$$

$$= P_{k+1,k}^1 \otimes P_{k+1,k}^2 \tag{3.9}$$

where the symbol $\otimes$ designates 2D convolution. The numerator of (3.4) is joint probability matrix $D_{k+1,k}^l$ defined for customer l with elements

$$D_{k+1,k}^l[i,j] = Pr\{d_{k+1}^l = j, d_k^l = i\} \tag{3.10}$$

$$= Pr\{d_{k+1}^l = j | d_k^l = i\} Pr\{d_k^l = i\} \tag{3.11}$$

$$= D_{k+1|k}^l[i,j] P_k^l[i] \tag{3.12}$$

Thus the entire $A_{k+1|k}$ matrix is computed with 1D and 2D convolution operations by

$$A_{k+1|k} = (diag(P_{k+1|k}^a)^{-1} (D_{k+1,k}^1 \otimes D_{k+1,k}^2) \tag{3.13}$$

3.4 Computing Aggregate Transition Matrix with FFT

An operation equivalent to the 2D convolution is computed in the frequency domain using the fast Fourier transform (FFT). Specifically, the 2D convolution of two 2D matrices in the spatial domain is equivalent to computing the FFT of these matrices and then the elementwise product of their frequency domain counterparts. Taking the nonnegative real part of the inverse FFT gives the same result as a 2D convolution in the spatial domain [81] [16]. The FFT runs most efficiently on matrices sized according to powers of two. After padding the square input matrices from their initial size to the next power of two in both dimensions, a PLASMiS pre-processing script aggregates the matrices pairwise for efficiency until the total desired aggregate count is reached. Runtime tests in MATLAB demonstrate the FFT method with this pairwise aggregation runs more efficiently than the equivalent with 2D convolution. For these reasons PLASMiS computes aggregate loads by adding sample paths from the component aggregates, each representing a customer count that is a power of two. For example, an input of 20 customers would be generated from summing sample paths of 4-customer and 16-customer aggregates. In this way PLASMiS computes aggregate Markovian loads using FFT in MATLAB/Simulink.

3.5 Modeling Load Clipping

The EM is a controller for the entire microgrid that sends and receives signals with the installed smart meters. Along with setpoints for dispatchable generators, the EM decides and sends the command when clippable loads should be clipped or the system's power cut. While a load goes to 0 when cut, its clipped value depends on the unclipped value and a constant load limit L. In this dissertation's case studies, clipping is a binary operation. In the clipped state all clippable loads are clipped, whereas in the unclipped state no loads are clipped. Furthermore, the case studies model one tier of clipping (i.e., the same constant clipping limit applied to all clippable loads).

This dissertation defines the action of clipping as either **(1)** leaving the unclipped sample value unchanged by clipping if it is between 0 and L or **(2)** bringing the clipped value exactly to L if the unclipped sample is above L. As with the unclipped load RV, the clipped load RV can

be characterized by a PMF (e.g., $P^{d^{ci}}_{k+1|k}$). The clipped load PMFs are zero for all values above L. As with unclipped loads, each RV of aggregate clipped loads is the sum of all individual clipped load RVs being aggregated. Similarly the value of each aggregate clipped load RV is sampled from its aggregate clipped load PMFs, calculated as the one-dimensional convolution of all the individual clipped load PMFs.

3.5.1 Precise Computation of Clipped Aggregate Loads

To incorporate dependency on the past state a Markov model can be implemented for each load, as introduced in Chapter 2, section 2.5. For the following discussion of an individual load, simplified notation is used without the load index i. At first glance an implementation of Markovian decision making between clipped and unclipped states requires transition matrices for each potential switch between states (unclipped to clipped and clipped to unclipped) for each k to $k+1$ transition. Markov transition matrices conditioned on the previous clipping state can be created from the joint probability distributions $P(d^c_{k+1}, d_{k+1}, d^c_k, d_k)$. The transition matrices can be constructed by summing over the entries not at play in a given transition (e.g., summing over d_k and d^c_{k+1} when going from the clipped to unclipped state, d^c_k to d_{k+1}). The conditional probabilities can be computed as follows.

$$P(d^c_{k+1}, d_{k+1} | d^c_k, d_k) = \frac{P(d^c_{k+1}, d_{k+1}, d^c_k, d_k)}{P(d^c_k, d_k)} \tag{3.14}$$

The calculation of $P(d_{k+1}|d^c_k)$ provides an example of how probabilities with clipping state transition can be calculated.

$$P(d_{k+1}, d^c_k) = \sum_{d^c_{k+1}, d_k} P(d^c_{k+1}, d_{k+1}, d^c_k, d_k) \tag{3.15}$$

$$P(d^c_k) = \sum_{d_{k+1}, d^c_{k+1}, d_k} P(d^c_{k+1}, d_{k+1}, d^c_k, d_k) \tag{3.16}$$

$$P(d_{k+1}|d^c_k) = \frac{P(d_{k+1}, d^c_k)}{P(d^c_k)} = \frac{\sum_{d^c_{k+1}, d_k} P(d^c_{k+1}, d_{k+1}, d^c_k, d_k)}{\sum_{d_{k+1}, d^c_{k+1}, d_k} P(d^c_{k+1}, d_{k+1}, d^c_k, d_k)} \tag{3.17}$$

In this way, each time step's load PMF depends on the previous load value and whether that load value occurred in a clipped or unclipped state. After calculating the conditional probabilities

characterizing the load change at each change of clipping state, sample paths for demand can be constructed within each simulation run.

3.5.2 Estimating Clipped Aggregate Loads for Computational Feasibility

The above-described method of constructing all possible sample paths offline, for each Monte Carlo iteration before the microgrid model is run, has a computational expense that becomes exponentially greater when the possibility of a discrete state change is added, e.g., to model clipping. Once probabilistic loads are aggregated for computational tractability, the individual load levels are no longer tracked. Tracking of the aggregate alone introduces the problem of uncertainty as to how much an aggregate load will be reduced by clipping the individual loads to a power limit. Since clipping is employed to reduce load and prevent a power cut, the benefit from clipping (i.e., the level of load reduction achievable) is important for simulations. Computations of clipping benefit in the best case (maximum load reduction) and worst case (minimum load reduction) follow below, with simplified notation for clarity. Since clipping benefit at k is computed from sample unclipped load at k with no time transition, the simplified notation excludes the time subscript (k, $k+1$, etc.). Without loss of generality, given q independent RVs for the individual unclipped loads, indices are assigned to order the loads by increasing value, i.e., $d^1 \leq d^2 \leq \ldots \leq d^{q-1} \leq d^q$.

Simplifying the notation of (2.6), a is defined as the aggregate unclipped load of q customers, the sum of $d^i \forall i \in [1:q]$. Each individual load value d^i falls within nonnegative constant bounds $\underline{d}$ and $\overline{d}$, i.e.,

$$\underline{d} \leq d^i \leq \overline{d} \tag{3.18}$$

Each load value d^i is clipped to value

$$d^{ci} = min(d^i, L) \tag{3.19}$$

where L is the constant, nonnegative power limit imposed on each load by clipping. The sum of all q clipped loads constitutes the clipped aggregate load

$$a^c = \sum_{i=1}^{q} min(d^i, L) \tag{3.20}$$

When a is sampled from aggregate probability distributions, individual d^i values are not tracked. This provides benefits of faster runtime and reduced complexity of Simulink inputs, but without individual loads tracked to compute individual and aggregate clipped loads. To characterize the clipped aggregate load a probabilistic model is therefore constructed. To estimate clipped aggregate a^c for a given a value, we calculate the maximum and minimum levels of load reduction ($a - a^c$) that can be achieved by clipping over all possible distributions of individual, unclipped load values that could sum to the given unclipped aggregate value of a. The value of L and the time-of-day dependent, unclipped aggregate load (computed in Sections 3.3-3.4) are given for the following computations of aggregate clipped load.

Maximum Load Reduction from Clipping (i.e., Best Case)

The maximum load reduction from clipping aggregate load, i.e., the best case result of clipping, is found by maximizing the quantity $a - a^c$. Since a is constant, this maximum load reduction corresponds to minimizing a^c. By the definition of a^c in (3.20), the combination of individual loads that produces maximum aggregate load reduction from clipping is calculated by the following minimization problem.

$$\begin{aligned} \min_{d^1,\ldots,d^q} \quad & \sum_{l=1}^{q} min(d^l, L) \\ \text{subject to} \quad & a = \sum_{l=1}^{q} d^l \\ & \underline{d} \leq d^l \leq \overline{d} \end{aligned} \tag{3.21}$$

Within the quantity to be minimized, the load limit L is constant so only the unclipped values below L (i.e., all $d^i < L$) are reduced by clipping. Thus maximum reduction by clipping will follow for d^i values that satisfy the following maximization problem.

$$\begin{aligned} \max_{j,d^1,\ldots,d^q} \quad & \sum_{i=1}^{j} d^i \\ \text{subject to} \quad & a = \sum_{l=1}^{q'} d^l \\ & \underline{d} \leq d^l \leq \overline{d} \\ & q' \leq q \end{aligned} \tag{3.22}$$

With optimal d^i values, the clipped aggregate load becomes

$$a^c = \sum_{i=1}^{j} d^i + (q - j - 1)L \tag{3.23}$$

The optimal (i.e., minimum) solution for load reduction due to clipping is $a - a^{c*}$ such that

$$a = m\underline{d} + d^{m+1} + (q - m - 1)\overline{d}$$

$$a^{c*} = m\underline{d} + min(d^{m+1}, l) + (q - m - 1)l$$

The load of unspecified value d^{m+1} can be divided as $d^{m+1} = \underline{d} + \delta^{m+1}$. Unclipped aggregate a then determines m and δ^{m+1}. For simplicity we define constant n as the number of maximized loads ($\overline{d}$), i.e., $n = q - m - 1$.

$$a = (q - n)\underline{d} + \delta^{m+1} + n\overline{d}$$

$$a = q\underline{d} + \delta^{m+1} + n(\overline{d} - \underline{d})$$

$$a - q\underline{d} = \delta^{m+1} + n(\overline{d} - \underline{d})$$

$$n = (a - q\underline{d})/(\overline{d} - \underline{d}) - \delta^{m+1}/(\overline{d} - \underline{d})$$

Since $\underline{d} \leq d^{m+1} \leq \overline{d}$, $0 \leq \delta^{m+1} \leq \overline{d} - \underline{d}$. Thus

$$\frac{\delta^{m+1}}{\overline{d} - \underline{d}} \leq 1 \tag{3.24}$$

which simplifies n, the integer number of maximized loads, to

$$n = \left\lfloor \frac{a - q\underline{d}}{\overline{d} - \underline{d}} \right\rfloor$$

Unclipped load value d^{m+1} is then computed $d^{m+1} = a - m\underline{d} - n\overline{d}$. Of the other individual loads, m take value $\underline{d}$ and $(q - m - 1)$ take value $\overline{d}$ while unclipped. This arrangement of load values

sums to a^c and is optimal (i.e., results in maximum $a - a^c$). We prove by contradiction for the two possible cases of how the aggregate load is shared between the individuals.

Proof $a - a^{c*}$ is the Maximum Load Reduction From Clipping

- **Case 1)** $m = j$ and unclipped aggregate $a = m\underline{d} + (q - m)\overline{d}$. The clipped aggregate is $a^c = m\underline{d} + (q - m)L$. We prove the optimality of a^{c*} by contradiction. We assume a^c is suboptimal (not the minimum given a), and we change an individual unclipped load to reduce a^c. Only the loads that exceed the minimum can be reduced, thus we reduce $(m+1)^{th}$ load from $\overline{d}$ to $d^{m+1} < \overline{d}$. Constrained by fixed aggregate constant a, one of the minimal loads of value $\underline{d}$ must be increased. The clipped aggregate becomes $a^{c'} = (m-1)\underline{d} + min(d^m, l) + min(d^{m+1}, l) + (q - m - 1)l$. Because $\underline{d} \leq d^m \leq d^{m+1}$, $a^{c'}$ is greater than a^{c*}. This results in a contradiction, and thus the assumption cannot hold. a^{c*} is optimal, i.e., minimized given a. Thus clipping benefit $a - a^c$ is maximized.

- **Case 2)** This more likely case has one individual load value d^{m+1} between extremes $\underline{d}$ and $\overline{d}$. The unclipped aggregate is $a = m\underline{d} + d^{m+1} + (q - m - 1)\overline{d}$ and the clipped aggregate $a^{c*} = m\underline{d} + min(d^{m+1}, l) + (q - m - 1)l$. As with case 1, we prove a^{c*} is minimal by contradiction. Assuming a^{c*} is suboptimal and can be reduced, we reduce d^{m+1}. To maintain the sum a, load m must be increased from $\underline{d}$ to $d^m > \underline{d}$. The clipped aggregate becomes $a^{c'} = (m-1)\underline{d} + min(d^m, l) + min(d^{m+1}, l) + (q - m - 1)l$. $a^{c'}$ is greater than a^{c*}. The only remaining option to adjust a^{c*} is to reduce one of the maximized individual loads from $\overline{d}$ to $d^{m+2} < \overline{d}$. Load d^{m+1} must be increased by the amount of the d^{m+2} reduction to maintain a, leaving clipped aggregate $a^{c''} = (m)\underline{d} + min(d^{m+1}, l) + min(d^{m+2}, l) + (q - m - 2)l$. Given constant a, clipped aggregate $a^{c''} = a^{c*}$. This results in a contradiction, i.e., a^{c*} is optimal and cannot be reduced given a. Clipping benefit $a - a^c$ is maximized.

Minimum Load Reduction from Clipping (i.e., Worst Case)

The worst case for clipping occurs with the combination of individual load values (unclipped) that yields the minimum load reduction from clipping. This load reduction $a - a^c$ is minimized

by maximizing a^c. The maximum clipped demand is calculated with the following optimization problem:

$$\begin{aligned} \max_{d^1,\ldots,d^q} \quad & \sum_{i=1}^{q} min(d^i, L) \\ \text{subject to} \quad & a = \sum_{i=1}^{q} d^i \\ & \underline{d} \leq d^i \leq \overline{d} \end{aligned}$$

The solution is

$$d^i = a/q \forall i \in 1:q \tag{3.25}$$

We prove by contradiction that the solution is optimal.

Proof Load Levels $d^i = a/q$ Provide Minimum Load Reduction from Clipping

For q customers, we look at all possible levels of clipped load. The customers are independent and each clippable to power limit L. RV a represents the aggregate load before clipping. Under clipping, each of the customers will be limited to consuming L (or left unchanged if already at or below L) once clipping is implemented. Depending on the values of $d^1, \ldots, d^q$ (before clipping), the benefit from clipping will fall in one of the following two cases:

- **Case 1)** $a \leq qL$. With each individual load at or below L, the aggregate load will not be reduced by clipping. One feasible solution that meets this criterion has the aggregate load evenly distributed across the q customers $d^1, \ldots, d^q = a/q \leq L$. No customer is above the clipped power limit so $a - a^c = 0$. Zero load reduction is by definition the minimum possible load reduction, since clipping DSM cannot create load (i.e., a negative load reduction is impossible from clipping).

- **Case 2)** $a > qL$. In this case, at least one of the customers is above the power limit before clipping is implemented. Thus clipping will always result in some positive load reduction. By the logic seen in the 2-house scenario, in the worst case here all customers are at or above L. Their clipped values are maximized (each equal to L) and the clipped aggregate is thereby maximized ($a^c = qL$). One feasible solution of this form similarly sees the load evenly distributed across the q customers $d^1, \ldots, d^q = a/q \leq L$. To prove by contradiction, we assume this solution is suboptimal and that changing individual load value(s) will increase a^c. We

move an individual load d^1 below L, which requires another load to increase such that the sum of loads still equals a. When clipped to L, this increased individual load will be reduced more than before the change, while the reduced load will remain unchanged at its lower value ($d^1 < L$) after clipping. The adjustment of individual values yields a higher load reduction under clipping and a lower resulting aggregate ($a^{c'} > qL$). With any individual load dropping below L the solution produces more reduction in clipping (less optimal) than the previously found solution. A contradiction, therefore the solution originally proposed (with all individual loads at or above L) is optimal. Thus the worst case clipping benefit is $a - a^c = a - qL > 0$. One solution of this form has the aggregate unclipped load spread equally between the individual loads.

Thus we have proven that for n houses, in both possible cases, a worst case solution (yielding minimum $a - a^c$) has the aggregate load equally distributed between all q customers.

3.5.3 Clipped Values Used in PLASMiS

The computations of minimum and maximum possible clipping benefit at each time step are implemented in PLASMiS to construct curves of estimated aggregate clipped loads. For the case studies in this dissertation, the estimate for clipped aggregate used in the simulator is the minimum possible clipped result averaged with the maximum possible clipped result. The EM similarly receives a computed estimate of aggregate clipped load, which the user can choose to be the minimum possible result, the maximum possible result, or some combination of the two. The EM uses this estimated value in a clipped state to allocate storage and dispatchable generation such that it meets the clipped aggregate load with little or no excess power generated. In a cut state, the EM uses the forecast of estimated clipped aggregate load to determine when storage and dispatchable generation are sufficient to bring the system back into a clipped state (i.e., meeting aggregate clipped load) and thus end the power cut.

Though the large loads (e.g., hospitals and factories) are kept unclipped in the case studies presented here, these large single loads can be tracked precisely when clipped. In a real world microgrid, the power levels of large loads would typically be known by the microgrid operator in clipped and unclipped states. For this reason they would not require their clipped load

to be estimated. In the PLASMiS EM, these large loads are sensed separately from the aggregate load, so large single loads can be known precisely in their clipped and unclipped states. Probabilistic quantities (loads and nondispatchable supplies) are assumed to be independent in PLASMiS, so the tool computes PMFs and transition matrices based on the aggregate RV formulae in section 3.3. The probabilistic quantities are then fed into the PLASMiS Simulink model as time-sequenced microgrid inputs, as described in Chapter 4.

A constant clipping limit L and fixed number of clippable homes make over-clipping common in the case studies, as shown in Chapter 7. If the percentage of clippable homes is too high or the clipping limit L too low, the decision to clip all clippable loads at certain times in the simulations are necessary to prevent cuts but overly conservative in the level of clipping. The clippable loads are reduced more than necessary in these cases of over-clipping, so energy that could be sold to willing customers is left on the table and the microgrid income is suboptimal. Extending the model to allow a dynamic clipping level is discussed as future work in Section 8.2.

Chapter 4

Modeling Islanded Microgrids

4.1 Introduction

The aim of scientific modeling is to approximate the physics of real-world systems, in this case real power distribution in a microgrid network. In this approximation the goal is to achieve technical accuracy while maintaining a reasonable level of computational efficiency, so hundreds to thousands of simulations can be run in a matter of minutes. To reach this balance, PLASMiS assumes each microgrid it models to be a single-bus, lossless, balanced power system that meets all reactive power requirements internally [67]. The single-bus assumption describes a distribution system that does not step voltage up or down, although transformers and related power electronics may be incorporated in the models of individual nodes in the network (e.g., in a generator model). These assumptions are made to facilitate a real-power-based model of a distribution network.

In the physical systems being modeled, clipping levels can be changed remotely by wireless communication. The clipping levels are based on customer preferences and microgrid inputs (weather conditions, equipment failures, etc.), as discussed in Section 2.3. The priority levels (specifying the order of dispatch) for dispatchable supplies and load clipping are also controlled remotely and can be easily changed depending on generator conditions and economics (e.g., fuel or battery storage prices). The EM in PLASMiS runs with different dispatch options that are enabled by this functionality, and PLASMiS can be used to quantitatively compare alternative dispatch strategies.

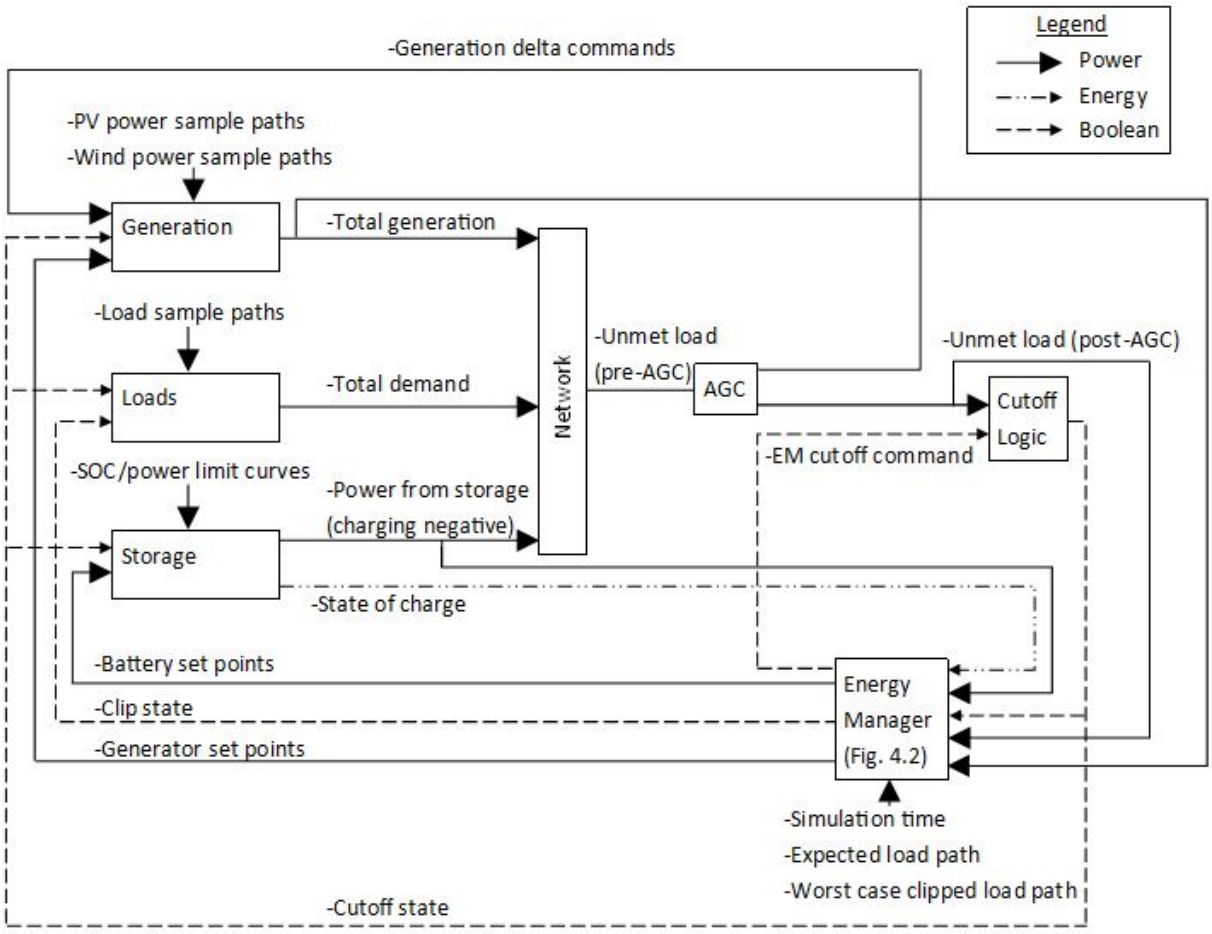

Figure 4.1: Simulink model schematic

PLASMiS supports the development of energy management strategies for microgrids that include fine-grained control of demand through smart meters at the residential load level [58], [61], [59]. Arbitrary combinations of loads, storage, and generation with orderings for dispatch and DSM can be constructed with control diagrams and functions in Simulink. The overall structure of the PLASMiS Simulink model is shown in Fig. 4.1. Each block in the figure is a subsystem containing the subsystem dynamics as well as the data input files required to run the simulation for a given set of data.

The Simulink models of the microgrid components are based on abstractions of more detailed models for the operation of each subsystem found in the literature [29]. Since the objective is to evaluate energy management strategies, details of fast transient dynamics are not necessary. We assume each subsystem is equipped with an internal control system and all the necessary elec-

tronics (e.g., current limiters and DC/AC inverters) operate stably and reliably in the modeled regime without performance degradation over time [33]. The following paragraphs describe the models comprising each of the Simulink components in the modeled microgrid network. The values used in Simulink for the case studies, and the sources of these values, are described in Chapter 6.

4.2 Loads

In PLASMiS, individual loads could constitute demand viewed at the granularity of specific appliances, but in the case studies individual loads correspond to buildings (e.g., homes, hospitals, businesses, and factories). Lighting and cell phone charging constitute the majority of loads in rural developing regions, and load clipping does not damage these devices as it could for larger appliances [18]. All loads in the modeled microgrids are assumed to be unharmed by load clipping to an arbitrary clipped power limit L.

The full demand in the microgrid model consists of clippable and unclippable loads. For the case studies, home loads d_k^l are added to unclippable larger loads (a hospital d_k^H and a factory d_k^F) as presented in Table 3.1. Summing Q total homes plus the larger individual loads produces total unclipped microgrid demand

$$a_k = \sum_{l=1}^{Q} d_k^l + d_k^H + d_k^F \tag{4.1}$$

where all three terms are Markovian and the $\sum_{l=1}^{Q} d_k^l$ term is computed as described in Section 3.3. If at k the EM's unclipped load forecast cannot be met, the clipped aggregate load is computed instead. Q^c is defined as the number of clippable homes of Q total homes. Indexing such that homes 1 to Q^c are clippable and homes $Q^c + 1$ to Q are unclippable, the total clipped system load becomes

$$a_k^c = \sum_{l=1}^{Q^c} d_k^{cl} + \sum_{r=Q^c+1}^{Q} d_k^r + d_k^H + d_k^F \tag{4.2}$$

If this clipped load cannot be met, a power cut results at k with no home loads being met, storage at zero charging or discharging power, and all generation cut to zero except backup

diesel generation, which runs only during power cuts to meet the hospital and factory loads

$$a_k^{backup} = d_k^H + d_k^F \tag{4.3}$$

While the microgrid is in a power cut state, PLASMiS compares the level of available supply against the EM clipped load forecast at each time step to bring the system out of a cut as quickly as possible.

As discussed in Chapter 3, the loads that constitute these aggregates are modeled as Markovian probabilistic quantities, so each one's sample value at $k+1$ depends on its value at k. Individual load RVs d_k^l can be aggregated for computational feasibility according to Sections 3.3-3.4. The sample values for these RVs, summed with the large load RV values, constitute the sample values for the aggregate RVs in (4.1)-(4.3). Each load is specified by a Markov transition matrix for each ten-minute time interval. As detailed in Section 2.5.1, these matrices are narrowed to PMFs and sampled to generate load sample values. From these samples taken every ten minutes, the Simulink model estimates power values at one-minute granularity by linear interpolation.

4.3 Nondispatchable Supplies

Nondispatchable supplies are driven by an external input (e.g., a natural resource) and are not controlled by PLASMiS. The external inputs are modeled as time-of-day dependent, non-Markovian probabilistic quantities as presented in Table 3.1, and these probabilistic inputs make the nondispatchable supply power levels probabilistic as well. The plant accepts any value received from a nondispatchable supply, since these supply values are nonnegative and driven by renewable resources without burning fuel. Thus the nondispatchable generation inputs are always considered beneficial and not limited by the network model in PLASMiS. Nondispatchable supplies are only curtailed in the case of a power cut, when all supplies are set to zero except backup fuel-burning generators. Nondispatchable supplies are not controlled in PLASMiS. Wind and PV are the two nondispatchable supply types modeled in the case studies. Both types depend on the weather in a given day. PLASMiS accounts for the weather-based differences by classifying each day-length simulation as either sunny, partly cloudy, or overcast and adjusting the level of solar and wind resources accordingly. Details of the weather considerations are described further in Section 6.2.

4.3.1 Wind Power Generation

Wind turbines constitute a nondispatchable supply producing power

$$s_k^w = \rho_W \pi R^2 v_k^3 C_P / 2, \tag{4.4}$$

with constants ρ_W the air density (constant 1.1839 kg/m^3 at sea level and T=25°C) and C_P the power coefficient (assumed constant 0.4). R is the constant turbine radius, selected as 1m. This is representative of small-scale wind turbines from commercial vendors such as Pika and Nature Power that range from 0.9m to 1.5m in radius and are rated for low wind conditions (less than 10 m/s, approximating wind speed in the proposed microgrid area in Rwanda) [4]. v_k is the wind speed at k, which PLASMiS samples every 10 minutes as a probabilistic quantity. As specified in Table 3.1, wind speed is sampled stochastically from PMFs that are independent in time (not a Markov model) but dependent on the time of day [59]. The wind speed data on which these PMFs are built in the case studies come from meteorological service Meteoblue, as discussed in Section 6.2. s_k^w is the power generated at k, which is provided to the Simulink model as a nondispatchable supply on a ten-minute basis. As with load, the Simulink model estimates power values at one-minute granularity by linear interpolation between the ten-minute power inputs.

4.3.2 PV Solar Power Generation

Similarly, PV panel output produces power s_k^{PV} given by

$$s_k^{PV} = \eta S I_k (1 - 0.005(T_k^{amb} - 25)), \tag{4.5}$$

where I_k is solar irradiance at k, T_k^{amb} the ambient temperature (°C) at k, S the array area, and η the system efficiency (assumed constant at 20%, a typical value) [34]. As with wind velocity, the Simulink model stochastically samples solar irradiance I_k on a ten-minute basis from time-of-day-specific PMFs. As listed in Table 3.1, these PMFs are independent-in-time and not Markovian. The PMFs are dependent on the time of day such that radiation ramps up then down with the arc of the sun and goes to zero between the times of sundown and sunrise [59]. The solar irradiance data on which these PMFs are built in the case studies come from meteorological service Meteoblue, as discussed in Section 6.2. Power output s_k^{PV} is provided to the Simulink

model as nondispatchable generation. As with wind power, the Simulink model estimates PV power at a one-minute granularity by linear interpolation between the ten-minute power inputs.

4.4 Dispatchable Supplies

Dispatchable supplies are commanded to a certain power output within a defined range by a microgrid manager, EM, or secondary frequency control system in PLASMiS. Supplies classified as dispatchable include gas turbines, dieselgenerators, and hydropower [67]. PLASMiS computes and compares microgrid performance for different strategies of dispatching generation, storage, and load clipping. For rural microgrid scenarios and generator options of East Africa, few supplies are typically available (i.e., few physical generators). Given the remote, uncommercialized nature of the typical sites, the choice of supply technologies is also often limited. Generally one to three different dispatchable generation technologies (e.g., hydro, gas turbine, and diesel generation) are available in the region. Each installation having a small generation capacity means the cost of dispatch is essentially proportional to the volume of fuel burned and/or labor required for operations and maintenance (O & M). A fixed slope curve (cost vs. power output) for each generator provides a good approximation of that generator's cost to run. This approximation makes it straightforward to solve the optimization problem of ordering dispatchable generation for minimum cost. Specifically, doing economic dispatch at each EM sampling time is a strict ordering problem where all the generators are in fixed hierarchy due to their constant slope cost curves. Generator ramping limits do not affect economic dispatch in PLASMiS because the EM's sampling time is ten minutes, longer than the maximum one minute ramp-up or ramp-down time of the relevant dispatchable supplies (hydro, diesel, and battery discharging).

AC generators overheat and fail prematurely when they are routinely run below a machine-specific minimum power level (i.e., below a power bandwidth commonly specified by the manufacturer). Dispatchable generators (e.g., hydro and diesel) are therefore limited in their output capacities to be either off (zero output) or within a positive power bandwidth (between power limits $s^{i,min}$ and $s^{i,max}$ specific to generator i). The PLASMiS model assumes that hydro flow and diesel supply is plentiful, so the desired power between the minimum and maximum limits can always be generated.

The power output in the generator models is updated at each one-minute time increment k. The setpoint for each dispatchable generator i is decided by the EM and sent to the plant's generator model i at the EM time granularity (10 minutes in the case studies). Generator i's power output is then decided in the plant according to a simple selection function of form

$$SELECT(x, y, logical) = \begin{cases} x, & \text{if } logical = 1 \\ y, & \text{otherwise} \end{cases} \tag{4.6}$$

To determine the logical value used in (4.6) a second function is used.

$$NEQ(x, y) = \begin{cases} 0, & \text{if } x = y \\ 1, & \text{otherwise} \end{cases} \tag{4.7}$$

Calling (4.6) and (4.7), generator i's power output is set to

$$s^i_{k+1} = SELECT(s^{EM,i}_{k+1}, s^i_k + \Delta s^i_k, NEQ(s^{EM,i}_k, s^{EM,i}_{k+1})) \tag{4.8}$$

where $s^{EM,i}_k$ is the k^{th} set point from the EM, and $s^{EM,i}_{k+1}$ the set point for time $k+1$. Δs^i_k is the change in generator i's output commanded by automatic generation control (AGC), explained further in Section 4.6.

4.4.1 Micro Hydro

Power output from a micro hydro plant is designated s^h_k and computed according to (4.8). Hydropower in simple terms is the conversion of potential energy in water into kinetic energy used to spin a turbine, which in turn spins an electric generator. PLASMiS models small hydro plants as run-of-river systems without pumped storage but sufficient head and flow to be dispatched at will up to a rated max power output. The commanded hydropower setpoint is limited both by maximum and minimum rated power and by ramping limits that depend on the installed machinery (e.g., sluice gates that are adjusted manually or automatically).

For the case studies ramping is assumed to take at most 1 minute (the model's time step for plant operations) between 0 (generator off) and the maximum rated hydro output. For the case studies, the hydro plant is assumed to be equipped with an on-site dump load or diversion load

(e.g., heating coils [62]) common in East African micro hydro sites. This allows the plant output in PLASMiS to be set anywhere from zero to the maximum, i.e., the minimum limit is set to zero and no discrete on/off command is necessary for hydro. Even when load falls below what would be a real-world generator's lowest nominal power output the plant can still be run and all unused power released as waste heat into the air or water.

This flexibility to choose an arbitrary level of hydropower output up to a rated maximum with no penalty or modeled resource depletion introduces the possibility of running hydro constantly at its maximum power output. Rather than running micro hydro at maximum power unnecessarily and assuming it to be a zero cost generation source, PLASMiS ramps hydro output up and down as needed to ensure aggregate supply matches total load. This avoids generating unnecessary waste heat with overproduction of hydropower.

4.4.2 Diesel Generator

Power output from a diesel generator is designated s_k^g and computed according to (4.8). The diesel generator is modeled as dispatchable with a sampling time of one minute for conservative testing, to account for the machine inertia and governor control system [79]. As with micro hydro the diesel generator is assumed to be fully dispatchable (from zero to maximum rated power output if needed) within the sampling time, following given maximum and minimum power limits. Discussion of nominal sizing and choice of limits is given in Section 6.4. The PLASMiS Simulink model assumes fuel is available as needed.

4.5 Energy Storage with Batteries

Battery storage is modeled in both the EM and the plant as an energy reservoir model. Energy stored in the battery is calculated as a running sum of all charging and discharging steps [41]. To account for physical limits and to prevent overheating, the reservoir model assumes some constraints on flow (i.e., charging and discharging rates) [33]. The maximum charging and discharging are limited dynamically based on the instantaneous battery energy. The limits come from curves that relate the battery's state of charge (SOC) to the maximum feasible power input and output. These curves come from battery specifications published by industry and specific to

the battery chemistry (e.g., lead acid or lithium ion) [2], [3]. In the PLASMiS Simulink model, these max charge and discharge curves are referenced at each time step to limit battery power output based on the current SOC. This improves the accuracy of the EM when commanding battery setpoints while also using the battery setpoints to choose dispatchable generator setpoints and the DSM state (clipped or cut load).

In the plant, the power outputs are integrated over the discrete time steps to track battery energy. For each battery bank (index j) the power output at k is termed b_k^j. With constant plant sample time Δt of one minute, the battery energy B_{k+1}^j is equal to

$$B_{k+1}^j = B_k^j - b_k^j * \Delta t \tag{4.9}$$

Note the sign for the change in energy is negative since the sign of battery power matches the supplies. In other words, battery power is signed positive when the battery is discharging (acting as a supply) and negative when the battery is charging (acting as a load). The updated battery energy is sent to the EM to limit its battery power command, as discussed in the following paragraphs.

In the case studies, one lead acid battery bank is modeled to fit the battery applications most prevalent in East African power systems. Models of lithium ion batteries have been implemented and tested in prior case studies [59]. Switching between the two battery types or simulating microgrids with both types is straightforward in PLASMiS. The two battery chemistries differ in their charging rates, where the recommended rates are 2.5 to 5 times faster for lithium ion batteries [3]. For both battery types the extreme regions of SOC, 90-100% and 0-10%, necessitate slower charging and discharging, respectively [33].

Each battery bank power output b_k^j is specified at k by any level between the maximum charging rate (negative) and maximum discharging rate (positive), limited by the energy level B_k^j. Upper and lower energy thresholds are set thresholds are set in PLASMiS to limit charging and discharging, respectively. In the case studies, for example, a 10% SOC lower threshold is in place for the system to note when discharging should not be continued. This signals to the EM that charging is needed. It also reduces the incidence of operating the batteries at SOC extremes in order to extend their cycle life.

4.6 Network and AGC Models

As shown in Fig. 4.1, the power levels from the loads, storage, and generation subsystems feed into the network block, which sums instantaneous generation, storage, and demand to determine the difference between the generated power and the aggregate load, termed the system delta. The system delta is then allocated to adjust the total generation up or down to match the total load. This allocation is accomplished by adjusting each dispatchable supply that's currently turned on (nonzero output) through a model that approximates how AGC systems adjust power output by multiple generators [32]. A typical AGC system of secondary frequency control is based on droop characteristics for each generator, and unmet demand is served by adjusting the setpoints of dispatchable generation to shift the generator droop curves for full demand to be met at nominal frequency. Given the real-power-based model in PLASMiS, with no model of frequency, the AGC functionality simplifies to constant distribution factors that allocate unmet demand between the dispatchable supplies in fixed proportions.

The so-called AGC block (shown in Fig. 4.1) adjusts the commands for dispatchable generation, sending generator-specific power deltas to the dispatchable generator models. The power deltas from the AGC block are portions of the system delta, split between the generators according to constant generator-specific distribution factors. The generator subsystems in turn adjust their power outputs as allowed by their ramping limits and max/min output limits. If the system delta is negative, indicating oversupply, the running dispatchable generators will be accordingly decreased by the AGC block. This is consistent with real world AGC systems sending commands to reduce generation when generators start spinning faster (increasing inertial energy in the system) to absorb oversupply [45]. If the system delta is positive, the AGC block accordingly increases dispatchable generation. If the dispatchable generators' limits will not accommodate the full increase commanded by the AGC block, a nonzero value of unmet delta is fed into the cutoff logic block. An unmet delta with a magnitude above the positive maximum delta limit induces a power cut, which sends a state change signal to the EM and the plant models (load, generators, and battery storage).

4.7 Power Cuts

A cutoff signal results in zero storage output and zero supply except backup diesel generation for the few large loads. Consequently, no loads are met in a cut except those with backup generation. In the case studies the hospital and factory are equipped with backup generation. By the nature of building-specific emergency generators, backup supply is not managed by the EM but by the consumers that own the backup generator(s). As with energy sold using diesel generation, PLASMiS tracks the energy generated from backup diesel generation. Once the cutoff logic block declares a cut, the EM must then decide when the system can be brought back online from a power cut to the clipped state, a decision made according to the algorithm in Section 4.8.

4.8 Energy Manager

Every ten minutes the energy manager sends new supply and storage setpoints, as well as clipping and cutting states for the system, as summarized in Fig. 4.2. Whether or not a cut is in place, the plant measurements (cutoff state, clipped state, generator outputs, and storage levels) are sent to the EM subsystem to choose the next system states and setpoints. The EM estimates present demand by summing instantaneous generation, unmet load delta, and charging or discharging power from the battery storage subsystem. The EM computes an estimate of load using this estimate of actual load together with unclipped and clipped load forecasts (expected outputs from the load forecast PMFs for the upcoming load).

From this estimate of the next load, the EM subtracts nondispatchable generation to compute a forecast of unmet demand. The EM then chooses setpoints for the storage and dispatchable supplies to send this unmet demand to zero. If dispatchable supplies and storage meet this remaining demand entirely, the EM has no need to limit demand with clipping or a power cut. If unmet demand cannot be eliminated, the EM sends state commands for clipping or a power cut as needed. If the forecast for unclipped demand can be fully met, the EM commands the unclipped and uncut state. In short, the EM chooses setpoints for storage and dispatchable generation to prevent power cuts and avoid load clipping. PLASMiS allows different dispatch schemes to be evaluated and compared on how well they meet these goals and others (e.g.,

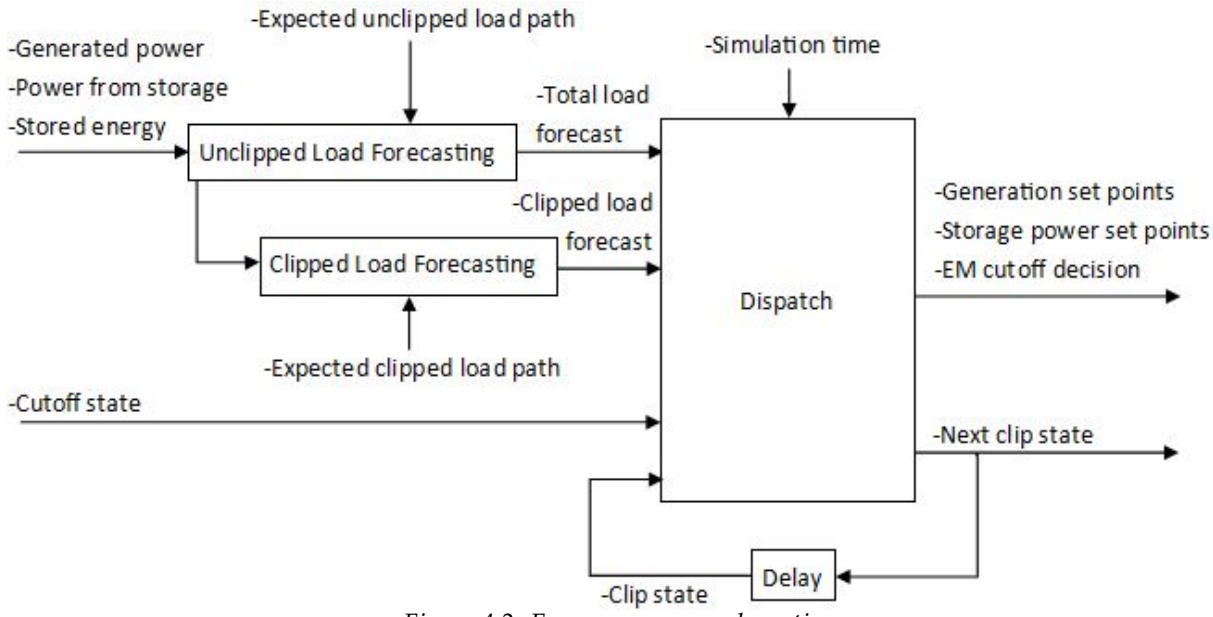

Figure 4.2: Energy manager schematic

reduction of fuel-burning generation).

In the dispatch step, dispatchable generation and storage are assigned setpoints every ten minutes in priority levels based on the time-dependent, state-dependent dispatch order set in the dispatch strategy block. The first priority supply option is dispatched first as needed to its maximum value, then the second priority supply, etc., until either the unmet load estimate for the coming time step is provided or all dispatchable generation and available discharging are allocated. The dispatch order and time-based limitations (e.g., on battery discharging) are changeable in PLASMiS, and the settings for this dissertation's case studies are as follows.

Hydropower is the first dispatchable supply option deployed at all times. The next resource dispatched is energy stored in batteries, provided the strategy allows for storage discharging at the given time (see case study 2). Finally, diesel generation is dispatched to cover any demand unmet by hydro and battery discharging. Once such priority levels are set for a specific microgrid design, dispatch order in the EM can depend on simulation time and the boolean state values for clipping and cutting, as shown in Algorithm 1.

Algorithm 1: Energy Manager Dispatch Scheme

```
net_unclipped_load=estimated_unclipped_load-power_pv-power_wind;
net_clipped_load=expected_clipped_load-power_pv-power_wind;
if discharge_allowed_flag(t) % storage discharge allowed then
    max_generation=max_hydro+max_storage_discharge+max_diesel;
else
    max_generation=max_hydro+max_diesel;
end
if max_generation < net_unclipped_load then
    bool_clip=1 % clip
    net_load=net_clipped_load;
else
    bool_clip=0 % unclip
    net_load=net_unclipped_load;
end
if max_generation<net_load then
    bool_cutoff=0 % Power cut, i.e., zero load met;
    Zero dispatch set hydro, diesel, and battery power setpoints to zero);
else
    bool_cutoff=1 % No power cut
    if discharge_allowed_flag(t) then
        Dispatch (in the following order) to meet net_load or maximize supply outputs
        1. Hydro
        2. Storage discharge
        3. Diesel
    else
        Dispatch (in the following order) to meet net_load or maximize supply outputs
        1. Hydro
        2. Diesel
    end
end
```

Lines 1-2 define the net load (clipped and unclipped) to be met by dispatchable generation and storage discharging. Depending on the clipping state the system demands, the EM will choose between these two quantities for the load to meet with dispatchable generation and storage. Lines 3-7 depend on boolean *discharge_allowed_flag(t)*, which equals one if storage discharging is allowed based on the time of day. If so, the maximum feasible discharge level (based on current SOC) is added to dispatchable generation, and together they constitute total available generation. If *discharge_allowed_flag(t)* equals zero, no discharging is allowed so total available generation is the sum of dispatchable generation (hydro and diesel in the case studies).

In lines 8-14, the EM determines if this total available generation will meet unclipped load, and if not the clipping state is set to one (i.e., clippable loads to be clipped). In this case *net_clipped_load* is set as net load for dispatchable generation and storage to meet. Otherwise the clip state is set to zero (i.e., all loads unclipped), and net load is set to *net_unclipped_load*. Lines 15-17 do the equivalent check to see if a power cut is necessary, and if so the cutoff state is set to zero (i.e., a system-wide power cut), as are all the dispatchable generation and storage setpoints. Lines 18-30 apply if no power cut is needed. The cutoff state is set to one (i.e., no power cut). Finally, the EM allocates generation and (if allowed) storage discharging to meet net load. The dispatch order can be arbitrarily defined by the user.

This algorithm prescribes that, except during a power cut, the EM seeks for each k to meet total unclipped demand from (4.1). The EM estimates this aggregate load through probabilistic demand forecasts adjusted according to an estimate of the most recent unclipped load. If the EM calculates it cannot meet unclipped demand, it seeks instead to meet the aggregate clipped load. If the EM calculates that available supply cannot meet its probabilistic clipped load forecast, then it sends the state signal for the microgrid to enter a power cut.

While the microgrid is in a power cut state, the EM checks its clipped load forecast at each sample time to decide if the system can be brought back online out of the cut. Throughout a power cut, the EM continues forecasting unclipped aggregate load and clipped aggregate load to maintain reference points for deciding when to end the power cut and what setpoints will be needed from dispatchable generation and storage immediately following a cut. If at any time during a cut the EM forecast in (4.2) can be met with available generation and storage, the EM returns the system to the clipped state and ends the power cut.

The outputs from the dispatch algorithm serve as system-wide state commands (for clipping and cutting) and as setpoints for the supply and storage subsystems in the plant. The clipping state applies fixed limits to clippable demand and adjusts supply and storage setpoints accordingly. The cut state sends the met load, supplies, and storage to zero one minute after cutting is commanded. With these state and setpoint commands the EM controls the load, supply, and storage subsystems described in this chapter.

Chapter 5

Simulation Tool

5.1 Overview

Developed in light of the context in Chapter 4, PLASMiS is designed to model a broad range of microgrid systems. PLASMiS is built in MATLAB and Simulink, since the latter provides a graphical interface for building simulation models that can be run in Monte Carlo simulation from MATLAB command files. Simulink is particularly useful for implementing control strategies based on real-time feedback from the dynamic elements modeled in the system being controlled. In PLASMiS the options of dispatchable generation and storage with clippable loads provide flexibility for control [67]. After offline pre-processing of inputs and sampling to construct paths for each load and nondispatchable supply, the Simulink model described in Chapter 4 is called for each Monte Carlo iterations, as summarized in Fig. 5.1. At each iteration the tool collects results from simulating the specified microgrid in operation and processes this data for diverse and practical metrics to evaluate microgrid performance. The data gathered is sent to the MATLAB workspace, saved, and analyzed in post-processing to compute metrics like energy sold and the lengths of clipping and power cuts.

Pre-processing is carried out in the MATLAB workspace to establish the input data for demands and nondispatchable supplies in all the Monte Carlo iterations. Next, the Simulink model is run once for each Monte Carlo iteration, using the respective inputs prepared in pre-processing. The Monte Carlo runs are managed by a MATLAB script that calls the Simulink model for each run and collects the simulation data in the MATLAB workspace for post-processing.

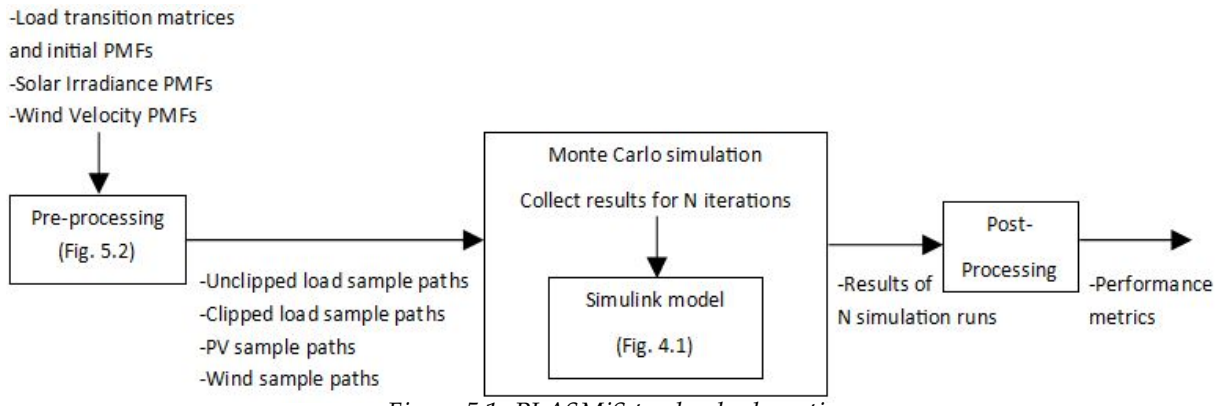

Figure 5.1: PLASMiS top level schematic

The post-processing step computes the metrics of interest using data from the entire set of simulations [58], [61], [59].

5.2 Pre-Processing

Pre-processing performs the steps shown in Fig. 5.2. A simulation data file loads constant initial conditions, generation and storage limits, sample times, and signal hold lengths into the MATLAB workspace. Constant time-sequenced distribution parameters are also specified for the probabilistic quantities (loads and nondispatchable supplies). From these parameters the pre-processing script generates PMFs and (for Markovian quantities) transition matrices for each time step. Small loads undergo the load aggregation step, where clippable and unclippable demands are aggregated separately. Large loads are kept individual to be tracked outside an aggregate, as a microgrid would desire for a large customer who might be helpful for load shedding or other grid services on high demand days. Like large loads, resource distributions for nondispatchable supplies are constructed and kept separate from each other (not aggregated) for stochastic sampling.

For each of the probabilistic quantities in the system (whether aggregate or left individual), a dedicated script then generates a random sample path for every Monte Carlo iteration from the quantity-specific probability distributions. After sampling, clipped load is computed for the clippable aggregate demand, as discussed in Section 3.5. Nondispatchable supply power curves (e.g., wind and solar) are computed from the sampled resource levels. The banks of supply and

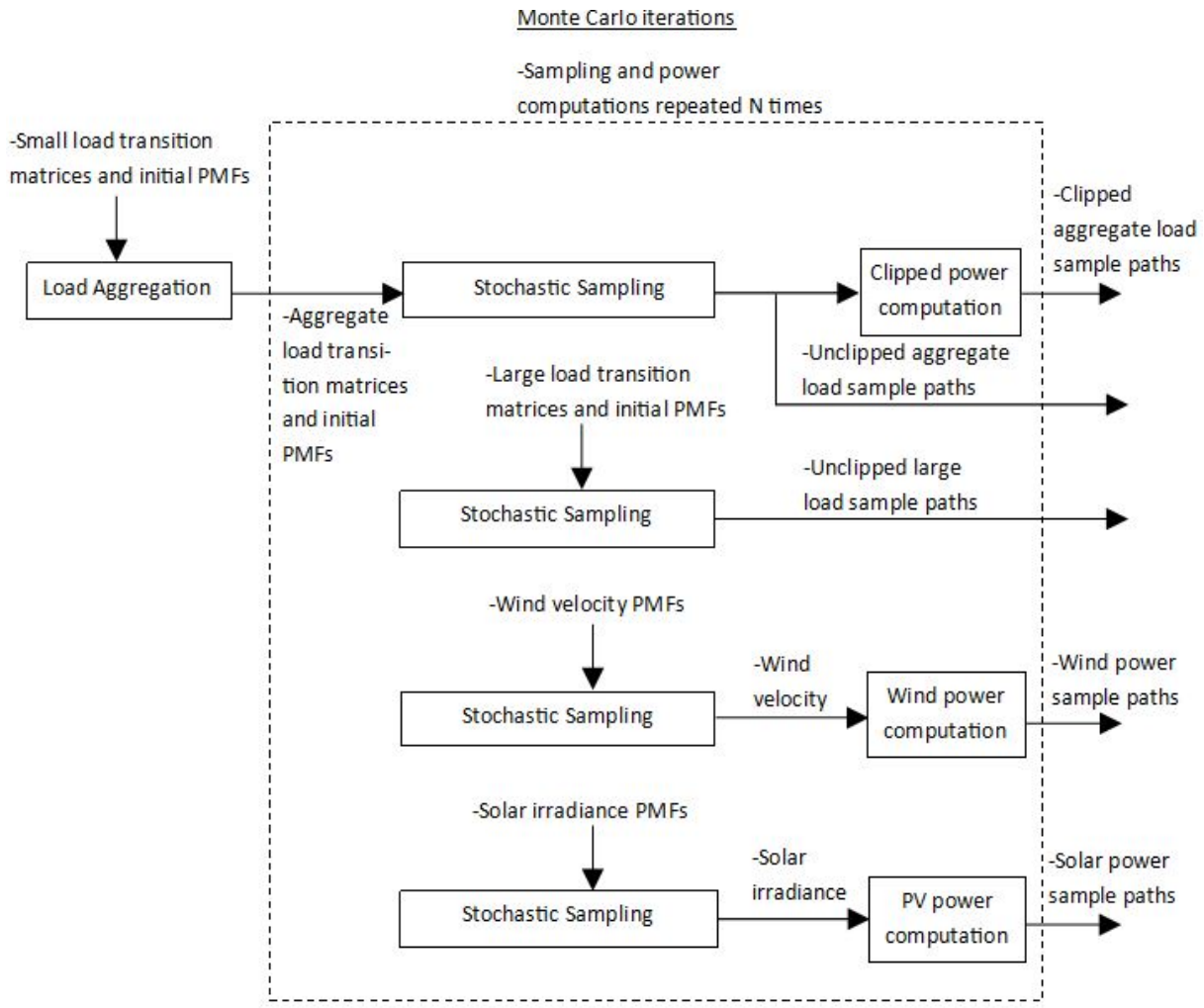

Figure 5.2: Pre-processing steps and inputs

demand sample paths are saved to run with different dispatch schemes and constant limits in the Simulink model. To test such a scheme, the power profiles are then fed into the Simulink model for Monte Carlo simulation.

5.3 Monte Carlo Simulation

After constant limits, initial conditions, and simulation inputs are generated in pre-processing, the Simulink model is run for a set number of Monte Carlo iterations. As discussed in Section 4.8, the Simulink model tests one dispatch strategy at a time. Probabilistic quantities do not depend on dispatch strategy, though dispatch decisions can cause them to be clipped or cut for certain time steps. Unlike the probabilistic quantities, dispatchable supplies and storage levels

are determined in the Simulink model at each run. Models of the specific subsystems in the Simulink model are described in Chapter 4.

For each Monte Carlo iteration, Simulink sends to the MATLAB workspace several types of computed data: demand levels, generation levels, storage levels (power and total energy), clip state, and cutoff state. In the MATLAB workspace, these data are logged according to the number of their Monte Carlo iteration and the simulation time step (corresponding to time of day in the case studies of this dissertation). On the supply side, these data generated in Simulink include the power levels of each type of generation over time, including backup generation deployed during power cuts (for loads with onsite backup generators). Similarly on the demand and storage sides, the power levels are recorded with any periods of clipping and cutting, and these data are also sent to post-processing.

5.4 Post-Processing

The post-processing step organizes and analyzes the data generated in Simulink. Data on the state of the network provide instances over time of demand clipping and power cuts. The post-processing calculations presented in this dissertation compute the length and variation of clipping and cutting instances over each 24-hour simulation period for the given microgrid configuration and dispatch strategy [59]. The computed metrics and raw data from Simulink are saved for further performance metrics to be computed in the future.

Chapter 6

Scenario for Case Studies

6.1 Introduction

For the case studies, the islanded distribution network being modeled and its input sizes are based on off-grid power systems in Rwanda. Supply technologies (PV, wind, hydro, and diesel generation) as well as storage type (12v lead acid car batteries) match what is available for purchase in the region. The loads also match typical demands in Rwanda, namely homes, a hospital, and a small manufacturing facility. This chapter describes the rationale behind the generation and storage sizing of the nominal system design to meet the aggregate load. The chapter concludes with testing the nominal design for the average sunny day case, when PV and wind are most readily available.

6.2 Factors to Choose Nominal System Design

Before generation and storage sizing is chosen for the case study microgrid, the load and a legacy power plant (hydro) are assumed to be in place. The details and sizing of these given components are described in Table 6.1, and these components with the desired additions are shown in Fig. 6.1.

The solar and wind resources change depending on the weather. To characterize the day-to-day weather in Kigali, Rwanda, PLASMiS uses city-specific weather data aggregated by Meteoblue from NOAA/NCEP measurements [5]. Meteoblue is a meteorological service spun out

Table 6.1: Sizes and types of given microgrid inputs

	Microgrid Component	Max Power (kW)	Type
Load	40 Houses	0.25/house, 10 in agg.	Markov load model
	Hospital	4	Markov load model
	Factory	4	Markov load model
	Micro Hydro Plant	15.5	Dispatchable

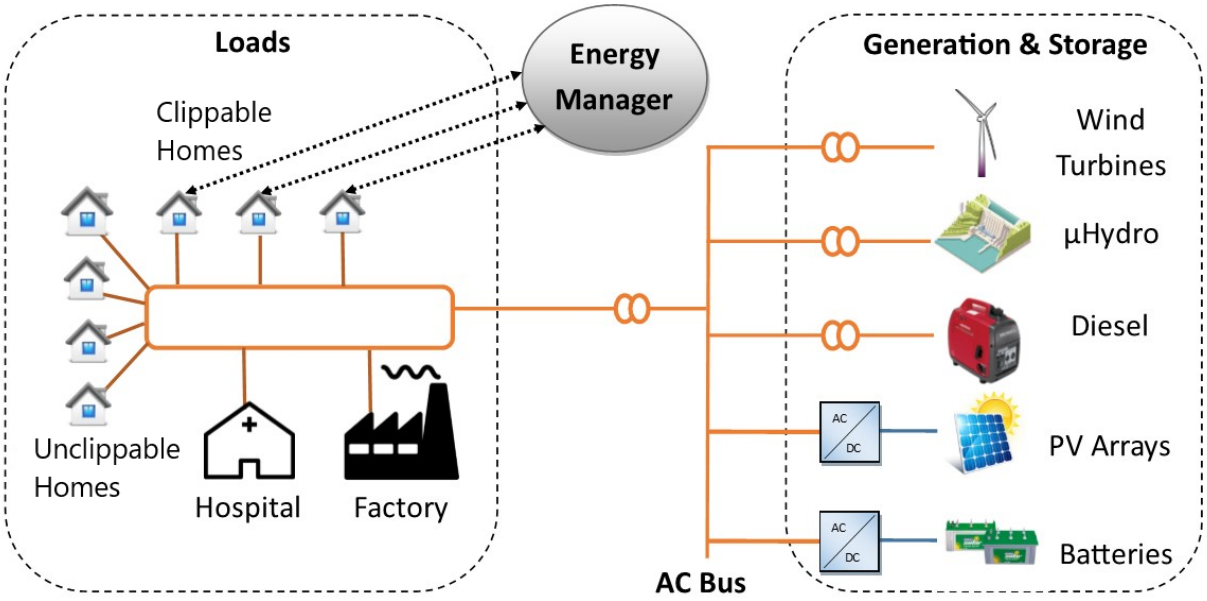

Figure 6.1: Schematic of microgrid component inputs for case studies

from the University of Basel to serve the agriculture, PV, and wind power industries. Meteoblue classifies days throughout a year as sunny, partly cloudy, or overcast, and then it gives the incidence and resource levels for each day type. Solar irradiance tends to be highest on sunny days, slightly lower on partly cloudy days, and lowest on overcast days, peaking around midday for all three weather types. Wind velocity similarly depends on weather and in Kigali tends to hover near its daily maximum between 10am and 6:30pm [7]. The numerical differences between these resource levels are reflected in the PLASMiS PV and wind models, and in pre-processing the fraction of days of each weather type is also specified. For Rwanda, with its two rainy seasons and two dry seasons annually, each year has on average 21% sunny days, 69% partly cloudy days, and 10% overcast days [7].

6.3 Demand

The load model aggregates 40 home loads plus one hospital and one factory load, as shown in Fig. 6.1. Average house demand is plotted in Fig. 6.2, along with maximum and minimum single house demand attainable from the Markovian distributions for each time of day. The two-peak load behavior follows roughly from models of weekday demand in [23]. In pre-processing,

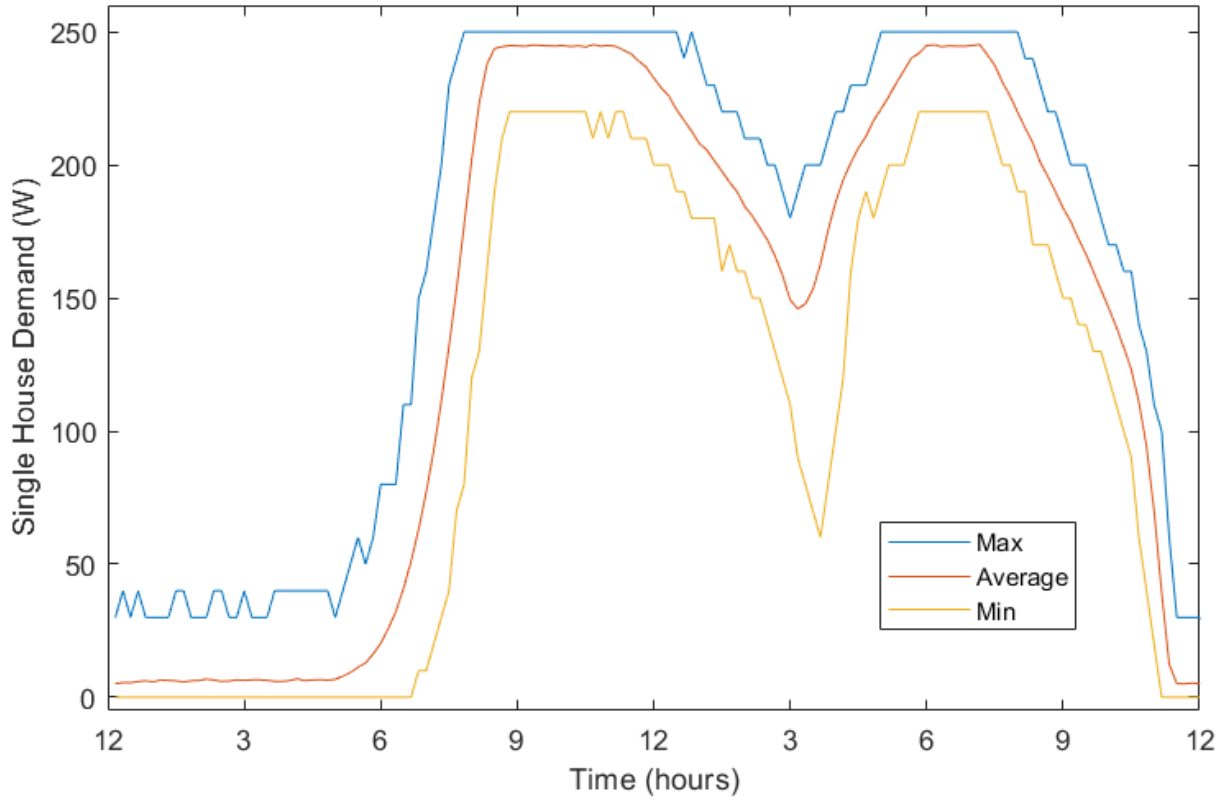

Figure 6.2: Maximum, minimum, and average load of a single house over one day

Markovian discrete probability distributions for each home load are aggregated and sampled for all Monte Carlo iterations as discussed in Chapter 3, section 3.3. In each iteration's call to Simulink, the hospital and industrial loads are added to the aggregate home load. The number of homes that are clippable by the EM is varied in different tests.

Average aggregate demand is plotted in Fig. 6.3. The hospital and industrial loads have maximum demands of 4kW each. The homes consume between 0 and 250W depending on the time of day, and clippable homes are assigned various clipped power limits L (in 10W increments) as commanded by the EM. The 250W peak demand for homes is based on the first-access energy

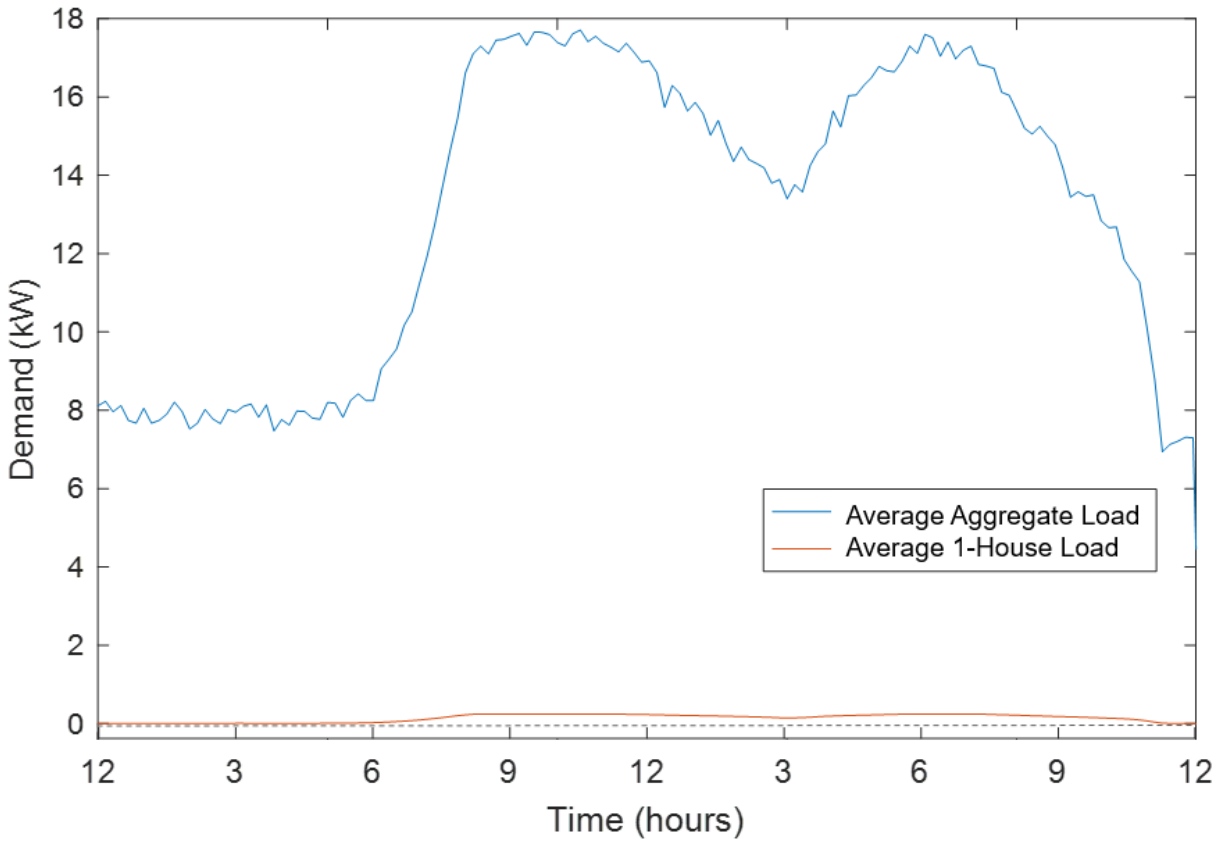

Figure 6.3: Average unclipped aggregate load (40 houses, a hospital, and a factory) over one day, with single house load plotted below for scale

capacity provided in Rwanda by German PV kit supplier Mobisol [46]. Mobisol sells 200W home systems that power a TV, a mobile charger, and 25 compact fluorescent light (CFL) bulbs [46]. Thirty watts was chosen as the minimum clipped power limit to test because this level is sufficient power capacity for home lighting and cell phone charging in newly electrified households in rural East Africa. The World Bank reports two CFL bulbs can be powered simultaneously with 24W [30], and 1-2 cell phones can be charged with the remaining 6W [52]. Furthermore, previous research with SparkMeter chose 30W as the lowest clipped power limit [18]. For comparison of operating strategies in the case studies, different numbers of houses are made clippable. In the case studies, the example microgrid is tested with the following different numbers of houses clippable: 32 houses (80%), 20 houses (50%), 8 homes (20%), and 0 homes.

6.4 Generation

The dissertation case studies model a microgrid with four supply technologies plus battery storage to meet time-dependent loads of multiple sizes throughout each 24-hour simulation. The chosen PV supply models an array of 10 Polycrystalline Silicon solar cells, similar to panels manufactured by BYD and used in Rwanda's first grid-scale solar installation [6]. Each panel has peak power output $W_p = 300W$ [1]. For the array as a whole this produces peak power output of 3kW at midday on a standard sunny day.

The wind supply has slightly lower capacity and is a model of 19 wind turbines similar to BONUS turbines examined in 2013 for installation in Rwanda [42]. Each turbine has peak power output $W_p = 150W$, a capacity matching the Rwandan government's pilot proposed in 2008 [64], [15].

The diesel supply models a generator rated to maximum 1kW output, with a minimum output of 0.5kW when turned on. The nominal output (upper limit) is selected to exceed the load unmet by hydro and battery discharging. The lower limit is selected as 50% of the upper limit to protect the generator from damage due to underloading [31]. This diesel generator size also matches previous research in PV-battery-diesel generation sizing for energy-poor African communities [22].

The largest generation source is a micro hydroelectric plant of maximum 15.5kW output, as discussed in Section 6. The plant is assumed to be a legacy installation where the size is given. This makes the addition of PV, wind, and diesel generation more economical for meeting the aggregate load than the alternative of expanding or adding hydroelectric capacity.

6.5 Storage

In PLASMiS, storage is modeled as a centrally controlled battery bank serving the entire microgrid, with no load having its own energy storage system. As such, storage has zero power output during power cuts. PLASMiS assumes no loss of charge when battery storage is sitting unused (neither charging nor discharging). Battery storage is modeled with two options for battery chemistry (lead acid and lithium ion), different levels of stored energy to start the simu-

lations, and multiple sizes for a battery bank. A model of 12V lead acid car batteries was chosen for the case studies to match the battery chemistry and individual battery size most commonly available for microgrids in East Africa and other developing contexts. Rather than maximum energy, charging and discharging rates (in units of power) became the limiting factor given the slower rates for lead acid as compared to lithium ion. Addressing this constraint when planning a real-world microgrid, practitioners advise oversizing a battery bank. They propose a maximum energy level high enough that the SOC will stay above 50% in daily operations [38],[80].

The number of 12V batteries in the battery bank model was chosen to provide 1.5kW of discharge capacity at a C-rate of 0.2, a common rate maintained by standard power electronics for lead acid batteries [20]. To meet these specifications the case study microgrid has a storage model of 250 batteries controlled as a single deployable storage resource. A hydro supply as sized above proves to be the primary generation source for charging battery storage, since the full hydro capacity is not needed in late night/early morning hours to meet demand. The battery SOC therefore stays near 100% from the simulated day's start time (12AM) until peak demand in the late afternoon and evening, when PV has dropped off. After the evening peak, hydro again charges the battery to nearly 100% by the end of the simulated 24-hour day. To mimic a real-world microgrid and ensure the simulation's ending SOC approximates its starting SOC, the SOC for the start of each simulated day is chosen to be near 100%, specifically 95%.

6.6 Nominal Design Sizing and Results for Average Sunny Day

The specifics of supply, demand, and storage sizing for the nominal system are detailed below in Table 6.2 and Fig. 6.4 to meet the load defined in Section 6.3. These sizes are chosen to provide sufficient power from generation and available battery discharging to meet the unclipped aggregate demand throughout the average sunny day in central Rwanda. Specifically, the maximum diesel generation and battery discharge power were chosen such that, when added to the maximum hydropower output, these supplies would exceed the demand unmet by nondispatchable supplies PV and wind. After subtracting PV and wind, the demand that remains is termed net load in Fig. 6.4, and this net load is plotted for both the clipped and unclipped cases. Overlaid across the net load curves are the stacked supply options at their maximum outputs. Note that

Table 6.2: Generation and storage specifications for nominal microgrid design

	Technology	Max Power (kW)	Type
Supply	PV Array	4.6	Nondispatchable (driven by resource)
	Wind Turbines	2.9	Nondispatchable (driven by resource)
	Diesel Generator	2	Dispatchable
	Micro Hydro	15.5 (given)	Dispatchable
Storage	Battery Bank	1.5 (discharge) 2.1 (charge)	120 kWh max energy Disharges (acts as supply) and charges (acts as load)

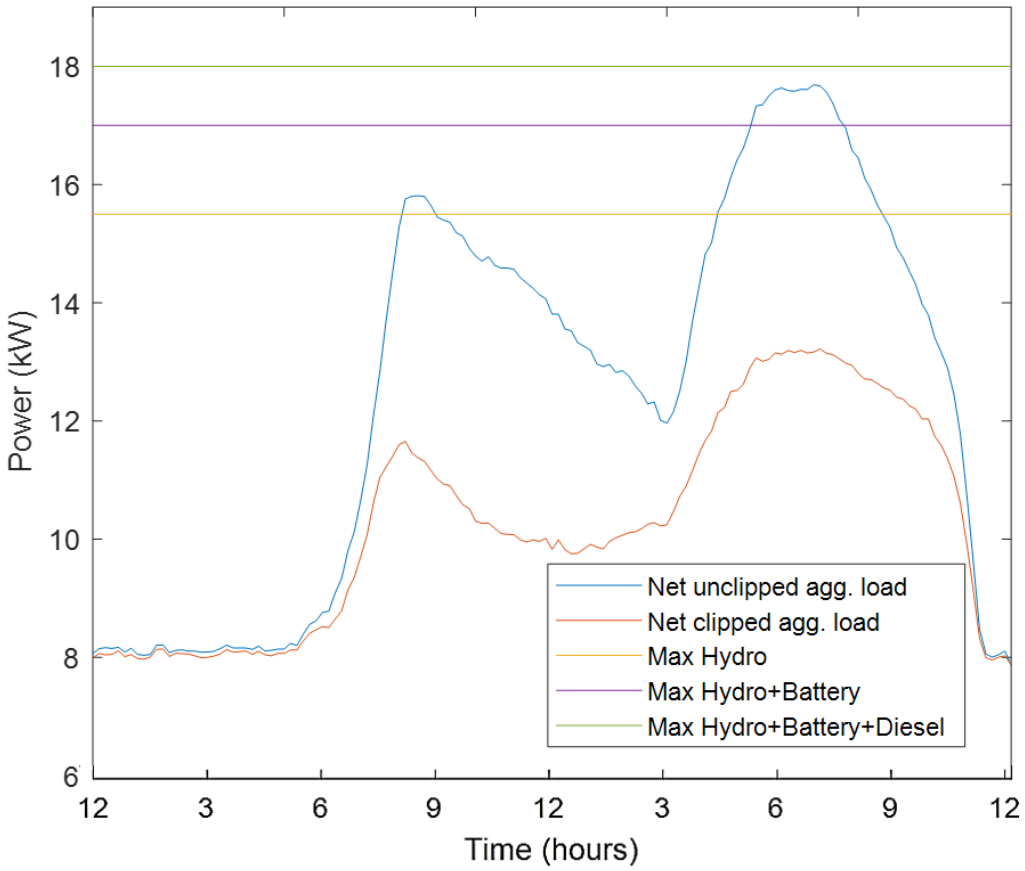

Figure 6.4: Net aggregate load (demand minus PV and wind power) on average sunny day, overlaid with maximum supply outputs

battery storage, for example, could not be run at this maximum constantly without periods of charging.

In the nominal system operations, 80% of the 40 homes are clippable (i.e., 32 clippable homes). Their clipped power limit $L = 150W$, from 250W maximum unclipped demand. This clipping rationale is reflected in the net clipped aggregate load curve, and this L value is also used in

Case Study 1 (Section 7.2).

The baseline test for PLASMiS with this microgrid scenario is the average sunny day's demand and nondispatchable supply levels modeled with the chosen sizes for generation and storage. As shown in Fig. 6.5 from testing on the average sunny day case, the supply and storage curves are not cut short by clipping or a power cut at any point. The nominal sizing is successful

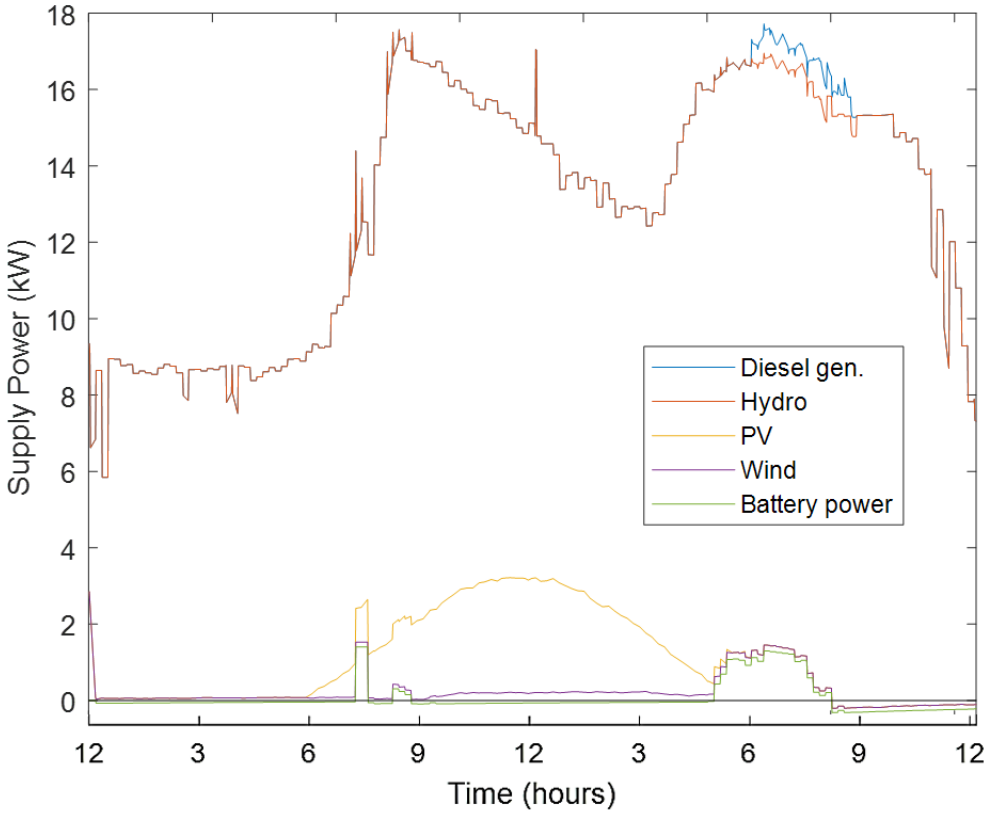

Figure 6.5: Generation and battery powers stacked to show total supply throughout the average sunny day

to avoid clipping and cuts on the average sunny day. Note that hydropower exhibits occasional peaks (e.g., around 12:30PM in Fig. 6.5) when it is the final dispatchable supply in the generation mix, as it is whenever the diesel generator is turned off. These unneccesary peaks result from imperfect load forecasting in the EM and conservative dispatching of hydropower.

As expected with the supply upper limits specified in Fig. 6.4, diesel runs for under two hours and only in the evening peak demand hours, when PV is unavailable. Because battery discharging is prioritized before diesel generation, the nominal microgrid design supplies less than 1% of the day's needed energy from diesel generation, as shown in Fig. 6.6. Overall the nominal design runs as expected for the average sunny day, since the EM meets unclipped load

throughout the day with little reliance on diesel generation.

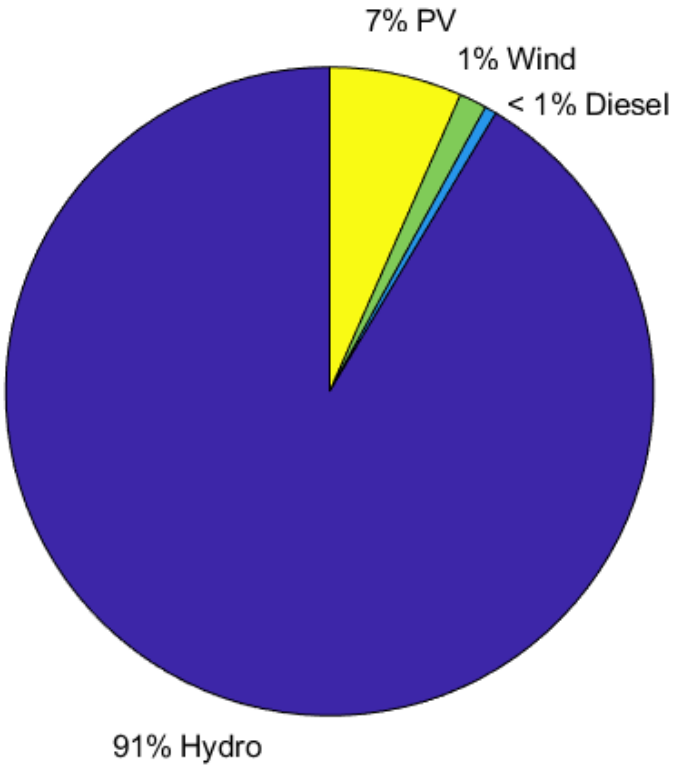

Figure 6.6: Breakdown of energy by supply technology on the average sunny day

Chapter 7

Case Studies

7.1 Introduction

Example applications of PLASMiS are demonstrated in the case studies. Testing for $N = 500$ Monte Carlo iterations shows the range of outcomes for 500 sample paths of each load and nondispatchable supply input, which vary across three weather types according to the seasons in Kigali. The 500 iteration count was chosen by a standard method of varying the number of samples (from thousands down to 100) and comparing the averaged results for each sample count. The sample count selected is the lowest for which the averaged results converge to within around 1% of the results from higher sample counts. This method produced the sample count of 500 when applied to testing microgrid operation strategies in PLASMiS.

The first case study below demonstrates how Monte Carlo analysis shows a wide range of performance for the nominal case, revealing state changes (clipping and power cuts) not discernible from the average day analysis given in Section 6.6. The second case study shows how varying the number of clippable loads affects the levels of energy sold and the likelihood of power cuts and clipping. The third case study explores the effects of changing the clipped power limit for a fixed number of clippable houses. The final study looks at adjusting both of the variables, clipped power limit and number of clippable houses, to demonstrate operational insights across two dimensions. Specifically, Case Study 4 aims to find the best operating point for a given performance metric, in terms of clipping limit and the portion of clippable loads.

7.2 Case Study 1: Monte Carlo Methods Applied to Nominal Design

The first case study entails further analysis of the nominal system that is tested on the average sunny day in Section 6.6. Specifically, Case Study 1 tests the nominal mode of operation with 80% of homes clippable to a 150W limit, and this Monte Carlo analysis results in no power cuts. The average outputs of generation and storage are plotted in Fig. 7.1.

From 9:30AM to 2:30PM the averaged hydro command signal chatters (see the red curve in Fig. 7.1). As expected, only the last supply dispatched has a chattering signal in such periods, and that last supply is hydro when diesel generation is off. Chattering in these simulations is due to imperfect load forecasting in the EM, which translates to hydro setpoints that are too low when aggregate demand is falling overall. The AGC subsystem corrects the imperfect setpoints and restores hydro output to its needed level in order to meet unclipped demand. The chattering behavior in the simulation results occurs because PLASMiS does not model the details of generator dynamics. In the generator's power output, the machine inertia prevents such quick spikes (<1 minute) from being implemented in practice. The hydro generator will therefore run according to the smoother, higher-output curve profile in these hours with the signals for lower setpoints coming every 10 minutes but not reducing the power generated to a level that could being total supply below aggregate unclipped demand.

Whereas the microgrid could meet full, unclipped load throughout the average sunny day with no clipping or power cuts, Monte Carlo analysis shows around one in five days require clipping with the nominal design, though always in short periods (typically fewer than 10 minutes of clipping per day). Fig. 7.2 shows the lengths of clipping for each of the 500 test days. While the longest clipping occurs on overcast days, as expected, clipping also occurs on occasional sunny and partly cloudy days. With probabilistic analysis, therefore, PLASMiS generates example sunny days where the supply is insufficient for unclipped demand. DSM is necessary even though the average sunny day required no clipping or power cuts with the same supplies and dispatch scheme. Table 7.1 gives the maximum, minimum, and average lengths of clipping for the days of each weather type. As explained in Section 6.2, 21% of days are modeled as sunny, 69% as partly cloudy, and 10% as overcast. Note from the minimum row in Table 7.1 that certain days of each weather types have no clipping or cutting at all. As expected, clipping on

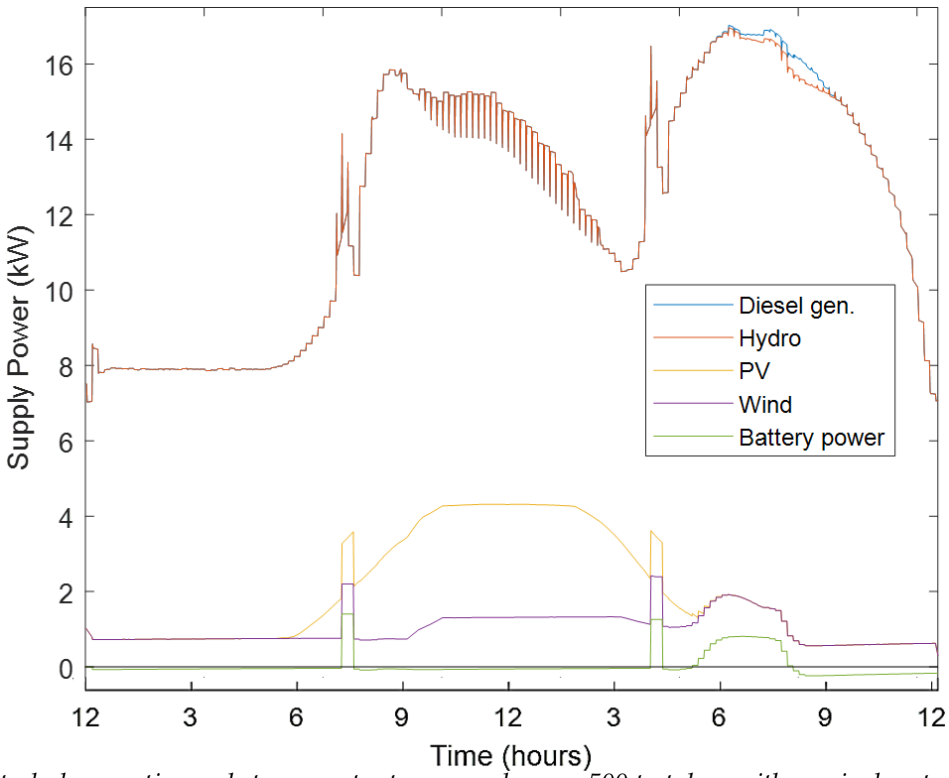

Figure 7.1: Stacked generation and storage outputs averaged across 500 test days with nominal system design (Case Study 1)

Table 7.1: Lengths of clipping in minutes/day for three weather types and overall(Case Study 1)

	Sunny	Partly Cloudy	Overcast	Overall
Maximum	10	10	40	40
Average	0.22	0.55	1.28	0.55
Minimum	0	0	0	0

partly cloudy days goes longer on average than on sunny days. On overcast days the average length of clipping is over twice the average on partly cloudy days. Fig. 7.3 shows the generation breakdown in terms of energy. The total clipping on any day is 40 minutes or less, with most days experiencing no clipping at all, so a grid operator may test reduced levels of clipping to increase energy sold, as discussed in Sections 7.3 and 7.4. Averaging across the 500 Monte Carlo iterations, energy from diesel generation remains below 1% of total energy. The portion of energy from PV and wind have increased when compared with the average sunny day results because both hydro and diesel output are usually reduced in clipped periods. PV and wind, by contrast, continue unchanged during clipping, with all of their power output used by the microgrid except

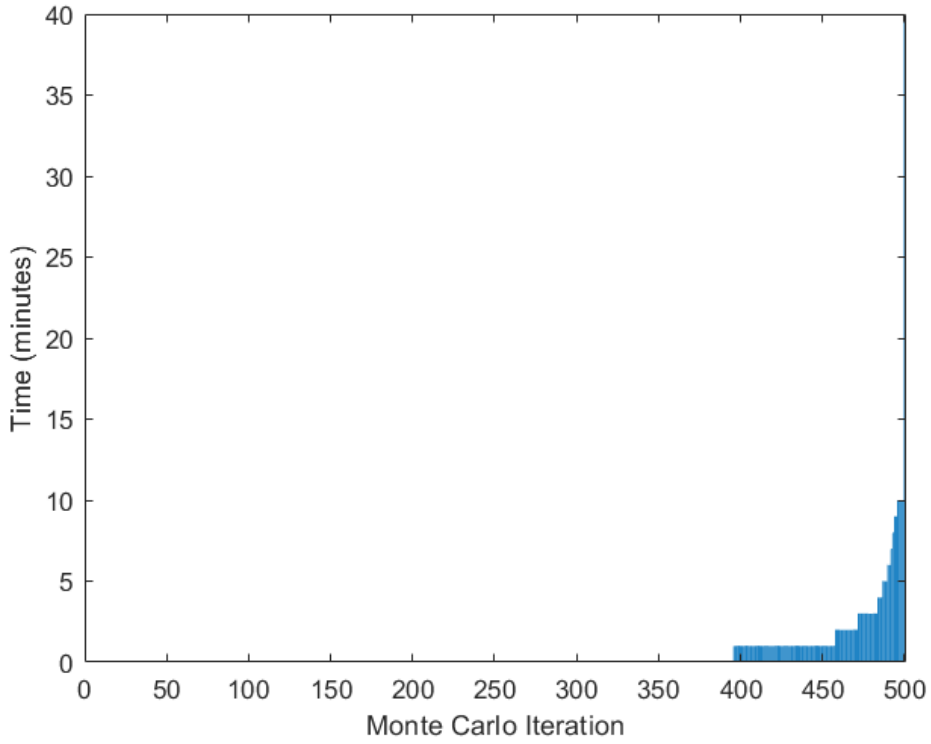

Figure 7.2: Lengths of clipping ordered from shortest to longest for Monte Carlo iterations with nominal design (Case Study 1)

during power cuts. These are some insights Monte Carlo analysis provides beyond the average day scenario by generating a range of energy and clipping/cutting outcomes.

7.3 Case Study 2: Varying Number of Clippable Loads

A microgrid operator or automated controller can choose different numbers of customers to clip depending on the limitations of the aggregate supply. In practice, utilities and microgrid operators communicate the clipping limit(s) to customers ahead of implementation. Utilities and microgrid operators alike communicate the clipping power limit(s) to affected customers, often providing the customers some compensation, e.g., lower electricity tariffs or a bill credit [11]. With sufficient clipping DSM the microgrid can serve its customers with reliable power, avoid power cuts by clipping low-tariff customers, and use limited supply to serve high-priority loads (e.g., hospitals, industrial loads, and security lights) [58].

To increase energy sold, the grid operator may decide to clip fewer customers and thereby

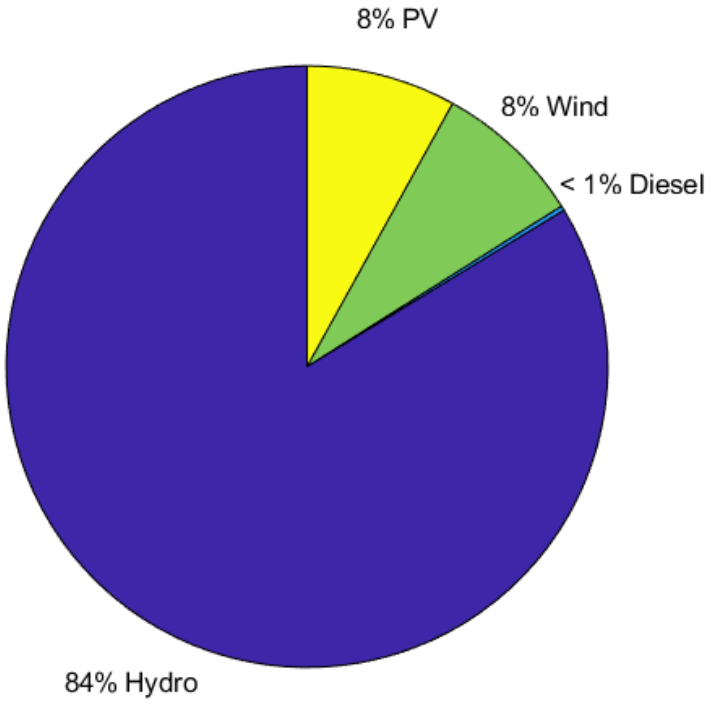

Figure 7.3: Breakdown of energy by supply technology over 500 test days for 150W clipping limit, 80% of homes clippable (Case Study 1)

limit fewer demands in the clip state. This case study looks at results of clipping 0, 20%, and 50% of houses. All of these scenarios are compared with the nominal design in which 80% of houses clippable. The clipping limit is kept constant at the nominal value of 150W for this case study. Simulations with 20% of homes clippable produce the average supply and storage curves in Fig. 7.4. In this average power plot a slight dip due to clipping is apparent from 6:30-8 PM in the hydro and diesel power curves, and then a further dip from cuts follows around 8-9 PM.

A comparison between the 20% and 80% clippable houses is shown in Fig. 7.5, presenting each iteration day's total time in the clipped or cut state. The nominal mode of operation with 80% of houses clippable (Case Study 1) results in no power cuts and a maximum clipping time of 40 minutes/day. Reducing the number of clippable houses decreases the aggregate load reduction from clipping. Clipping only 20% of houses causes certain high demand periods that required only clipping in the nominal case to now require power cuts bookended by periods of clipping. Fig. 7.6 presents the lengths plotted in Fig. 7.5(b), now separated into lengths of (a) clipping and (b) power cuts with 20% of homes. The maximum length of clipping in a day has risen to 28 minutes, and the maximum length of power cuts is 56 minutes in a day. While

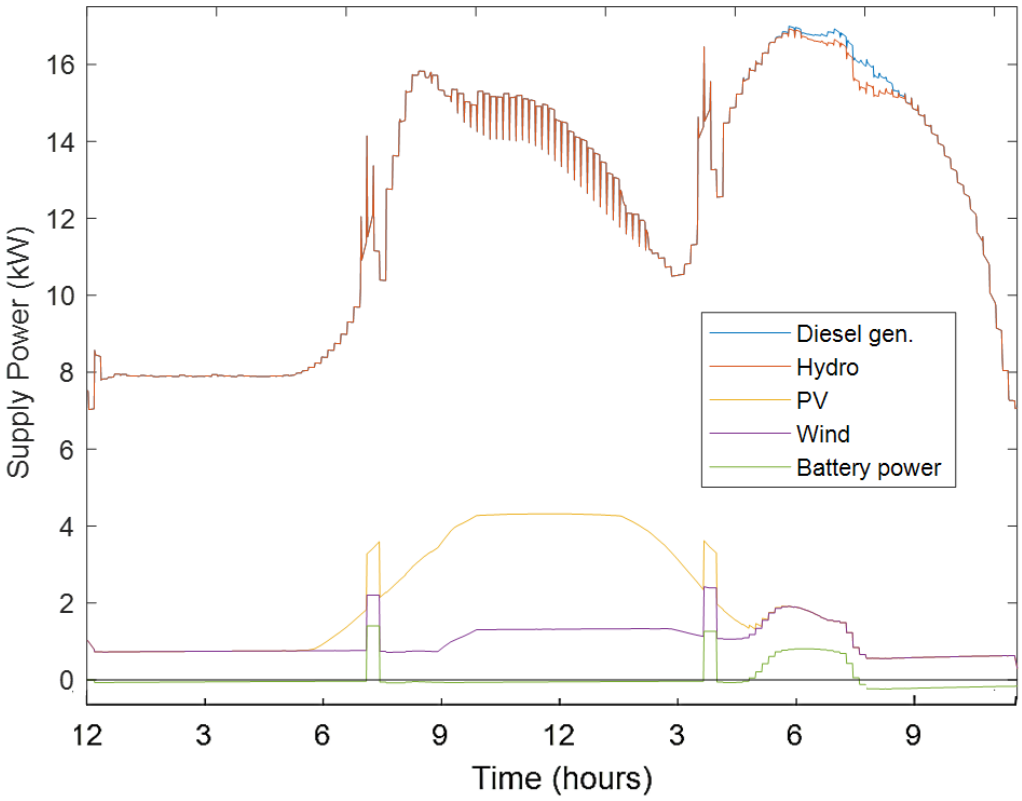

Figure 7.4: Stacked generation and storage outputs averaged across 500 test days with 20% of home loads clippable (Case Study 2)

diesel generation still produces under 1% of the total energy, and percentage breakdown of the generation technologies matches the nominal case (Fig. 7.3), the energy from diesel generation does increase. This rise results from operating backup generation during power cuts to supply the hospital and factory loads. Total energy sold goes down because the majority of consumers are cut entirely. Overall, reducing the number of clippable homes causes a degradation in quality of service and in the operator's bottom line. The cause is limited generation capacity and insufficient DSM intervention to reduce load when it exceeds available generation.

The case of no clipping has more drastic degradation, as shown in the clipping times of Fig. 7.7. On certain days the evening supply capacity (when PV is absent) becomes too small to meet unclipped demand. Power cuts last up to 124 minutes and occur on 6% of days. Dispatch of the full generation and storage assets in the test microgrid are insufficient to meet load on these days, i.e., the supplies are undersized for the demand and demonstrate the need for DSM. With no clipping capability, the reliance on diesel is also increased to 4% of the total energy (see Fig.

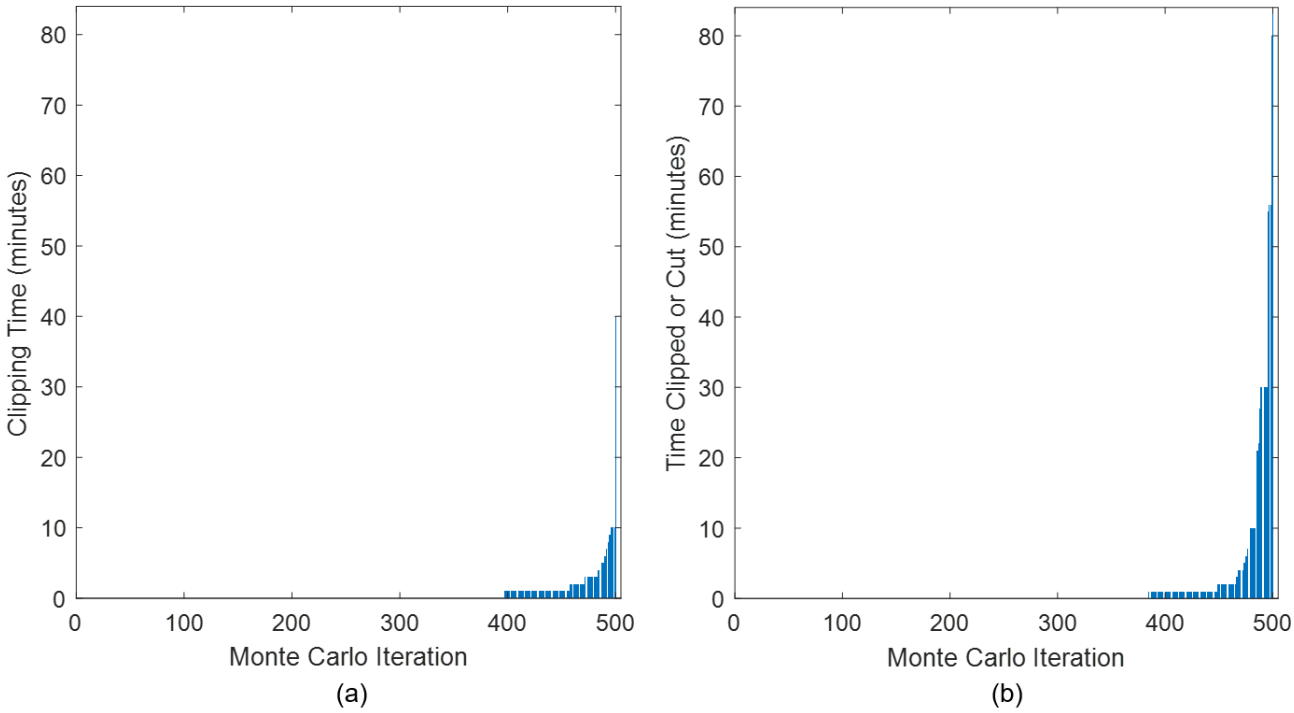

Figure 7.5: Length of time in the clipped or cut state with (a) 80% of houses clippable and (b) 20% of homes clippable, all to limit L=150W (Case Study 2)

7.8) and an average of 12.6 kWh generated daily from diesel (see Table 7.2).

The case of 50% clipping is also tested for comparison, and it confirms the following general pattern given a 150W clipping limit. As shown in Table 7.2, when 50% or more of houses are clippable power cuts do not occur and clipping times remain essentially constant. The final

Table 7.2: Clipping, cutting, and energy sold, variation by portion of houses clippable to 150W limit (Case Study 2)

		Percentage of Houses Clipped			
		0	20%	50%	80%
Clipping Time (min/day)	Maximum	N/A	28	10	40
	Average	N/A	0.9	0.5	0.6
	Minimum	N/A	0	0	0
Power Cut Time (min/day)	Maximum	124	56	0	0
	Average	2.09	0.8	0	0
	Minimum	0	0	0	0
Average Energy Sold (kWh/day)	Renewable	319.7	293.4	297.9	293.7
	Diesel	12.2	0.8	1.0	0.7

two rows of Table 7.2 document how energy sold decreases when more than 50% of homes

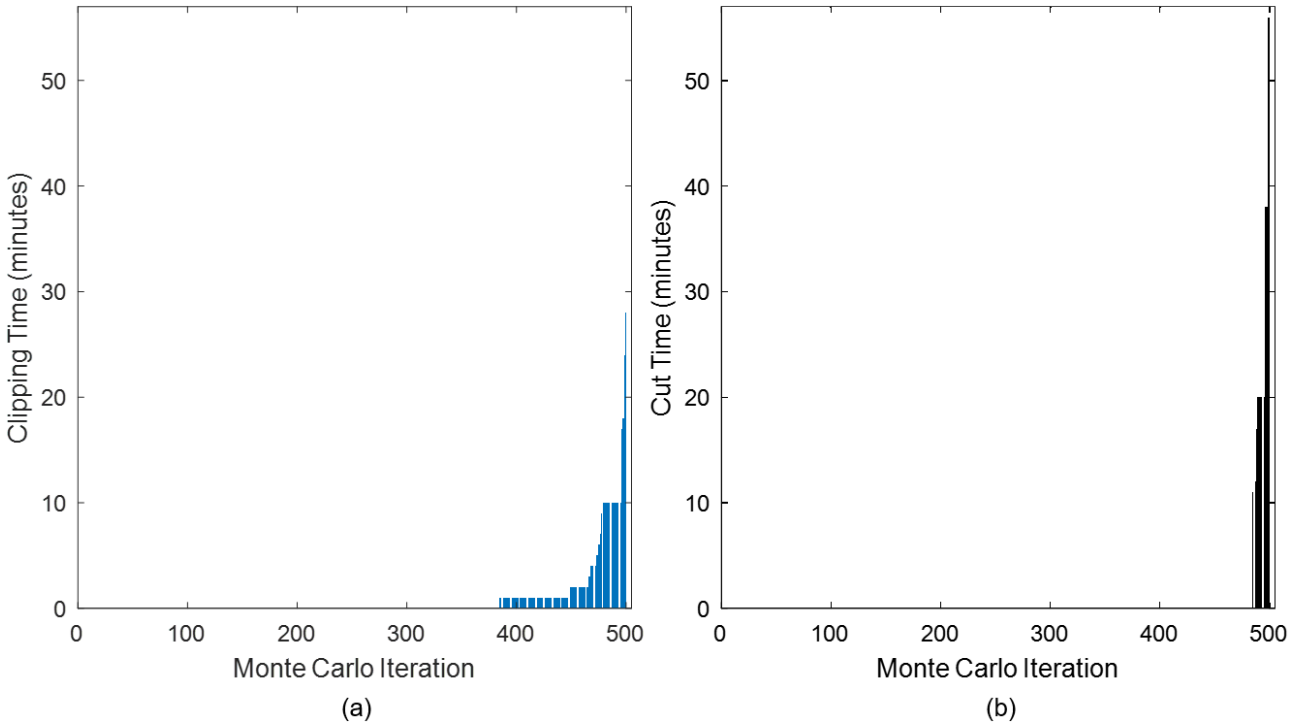

Figure 7.6: Length of (a) clipping and (b) power cuts ordered from shortest to longest for 20% of homes clippable to limit L=150W (Case Study 2)

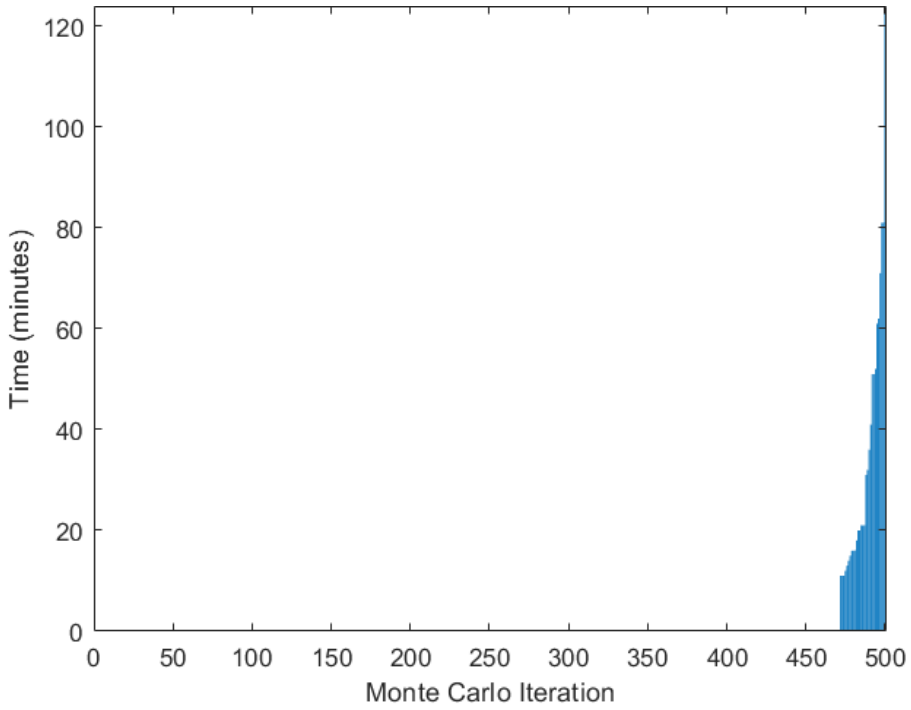

Figure 7.7: Length of power cuts ordered from shortest to longest for no loads clippable (Case Study 2)

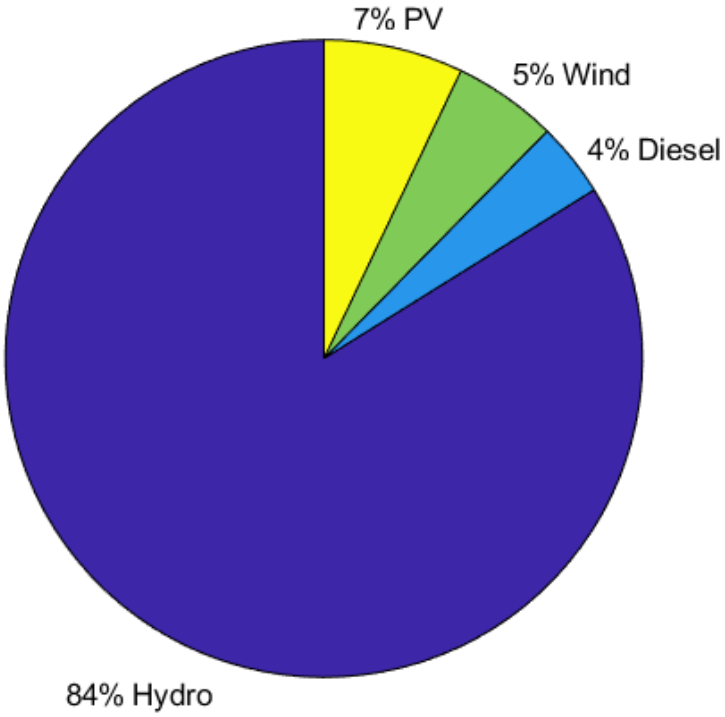

Figure 7.8: Breakdown of energy by supply technology over 500 test days with no clipping (Case Study 2)

are clipped. In other words, clipping 80% of homes to a 150W limit is over-clipping, and the microgrid operators in this case leave available energy unsold.

Energy sold peaks for the 50% clippable case, though at the same time energy from diesel generation is higher than cases of more houses clippable and less energy sold. The dispatch strategy in place, outlined in Algorithm 1, deploys diesel generation before clipping DSM, but a change in the EM could change these priorities to clip loads before burning diesel. In this case total energy sold would be reduced, but diesel generation would only be deployed to prevent a power cut or to provide backup power for high priority loads in the case of a general power cut. The monetary and environmental costs of burning diesel would be decreased, but with the tradeoff of reducing energy sold and potentially lowering customer satisfaction.

7.4 Case Study 3: Varying Clipped Power Limit

Grid managers experiment with changing the clipping limits for clippable homes to increase energy sold to those homes. As a test of such a change, Case Study 3 starts by examining the same microgrid operating with a constant clipping limit $L = 30W$ (rather than 150W nominal).

As with Case Study 2, 20% of the houses are clippable. With a 30W clipping limit no cuts result on any of the 500 days, since the 30W clipping limit reduces aggregate load sufficiently for the supplies and storage discharging to always meet clipped load. The longest clipping on any test day is 6 minutes, and as with the nominal scenario clipping only occurs on overcast days.

The third case study also looks at the clipping limits between 30W and 150W, aiming to increase energy sold to clippable customers. Table 7.3 presents the maximum, minimum, and average lengths of clipping and power cuts for each of the Monte Carlo iterations. The bottom two rows show total energy supplied with each different clipping limit in effect. To consider strategies where renewable generation is prioritized, the total energy is divided between renewable and diesel generation.

Table 7.3: Clipping, cutting, and energy sold, variation by clipping limit for 20% of homes clippable (Case Study 3)

		Clipped Power Limit				
		30W	60W	90W	120W	150W
Clipping Time (min/day)	Maximum	10	10	11	33	28
	Average	0.51	0.47	0.55	0.53	0.87
	Minimum	0	0	0	0	0
Power Cut Time (min/day)	Maximum	0	20	20	74	56
	Average	0	0.04	0.06	0.34	0.83
	Minimum	0	0	0	0	0
Average Energy Sold (kWh/day)	Renewable	293.4	296.8	293.5	296.7	293.4
	Diesel	0.8	1.0	0.8	1.0	0.9

This table shows that different conclusions emerge depending on the strategic goal. Given a fixed 20% of homes clippable, if the microgrid operator wants to assure fewer than one power cut each 500 days then 60W is the best clipping limit. If, however, the microgrid operator accepts occasional power cuts up to 20 minutes in length, statistically occuring once every 500 days, then the 90W limit is an improvement because energy sold is highest for this limit. The average clipping time per day is also low die 90W limit, with a maximum of 11 minutes daily clipping observed. Adjusting variables for the operator's specific goal is further discussed in Case Study 4.

7.5 Case Study 4: Two Variable Analysis

Mathematically choosing the best operational point in terms of multiple variables requires finding local extrema. One common approach to find local minimums and maximums involves adjusting the variables around a limited region in their value spaces. This region of focus is one that yields promising results from initial tests at a rougher granularity.

For the case study microgrid scenario, the metric chosen to rank options in this case study is average daily time the system is in the clipped or cut states. Priority is also given to options that yield zero power cuts over all the Monte Carlo iterations, and to maintain a high quality of service the least clipping that will accomplish the zero cut case is preferred. The clipping limit range of 90W to 220W for 50-80% clippable loads appears promising in light of prior case studies' results. Testing at a finer granularity within this region suggests to minimize average clipped or cut time without unnecessarily clipping customers the operating point should be a 90-180W clipping limit with 50% clippable homes. The surface in Fig. 7.9 shows this trough, where the 90W limit, 50% clippable pairing is optimal in terms of minimizing average time the system was either clipped or cut. Furthermore, this operational point had zero power cuts throughout Monte Carlo analysis. This optimal operating point is highlighted with the left white dot on the surface.

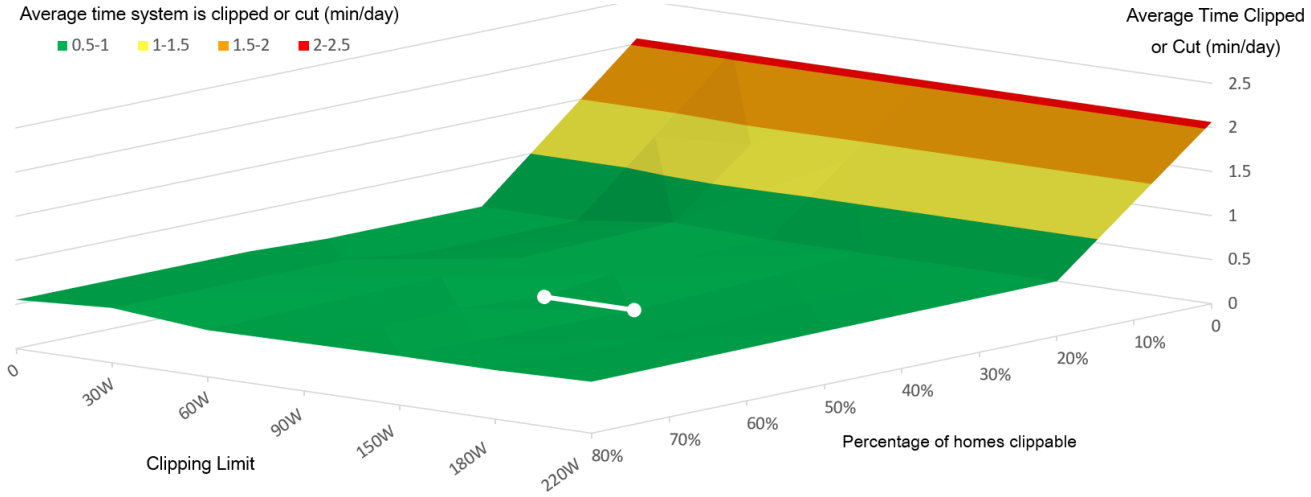

Figure 7.9: Average daily time in either the clipping or cut states, as affected by variation in clipping limit and percentage of houses clippable. Optimal operating points highlighted in white (Case Study 4)

Marginally worse for low average clipped or cut time is the connected right dot (150W limit, 50% of homes clippable). This operating point produces on average 0.01 minute more clipping per

day than the optimum, while on the metric of energy sold it performs better given the higher clipping limit. Clipping more than 50% of homes or clipping to a lower limit than 90W lowers aggregate load unnecessarily, which in practice could reduce both grid income and customer satisfaction.

The green area extending left from the highlighted white line along the percentage axis (i.e., scenarios of 50% or more houses clippable) constitute extremes of clipping that is unnecessary, and these operating points result in over-clipping. This nearly flat portion of the figure shows increasing the number of clippable houses does not reduce the average time in clipped or cut states. The increase in clippable homes over this range does, however, drastically decrease the energy sold to customers, thus reducing grid income. Similarly, clipping limits lower than 90W for the $\geq$ 50% clippable cases result in over-clipping based on the size and load variation of the case study microgrid. Performance in terms of minimizing time in the clipping or cut states does not drop even by moving the clipping limit lower or the clippable percentage higher than the optimum described. With results like this tailored to their specific microgrid scenario (whether built or in planning stages), microgrid operators can ensure they are not over-clipping and thereby leaving energy unsold. More specifically, they can identify the highest clipping limit(s) that will serve their operational goals and the minimum number of loads to clipped at a given time in order to meet those goals.

Chapter 8

Conclusions and Future Work

8.1 Summary of Contributions

This dissertation has presented background and applications surrounding PLASMiS, a probabilistic simulator for microgrids. PLASMiS evaluates microgrid operations and planning by quantitative metrics. The tool models microgrid inputs probabilistically and accounts for load clipping DSM from smart meters as an operational decision for energy management.

The contributions of this dissertation include derivations for probabilistic models, a rationale for modeling microgrid energy management, and results from this modeling approach. Regarding the mathematics, Chapter 3 gives derivations for aggregate transition matrices and PMFs to characterize a microgrid's probabilistic quantities as RVs. The aggregation step in pre-processing reduces computational expense and runtime for the microgrid simulation steps. These RVs are designated either independent in time or Markovian. Markovian loads are modeled in their unclipped and clipped states as dependent RVs, conditioned on the prior time step's sample value. Applying probability theory to bound and estimate load clipping DSM provides a Markovian approach to aggregate load modeling and intelligent dispatch of generation and storage.

The probabilistic nature of inputs in PLASMiS, discussed in Chapter 4, is one of its primary contributions to the microgrid simulation landscape. PLASMiS allows arbitrary, discrete probability distributions to characterize microgrid inputs at each time step, with or without Markovian dependency. This level of control over load characteristics, and the matrix-based method presented for aggregating load distributions, are enabled by the user-defined probability models

[59].

As demonstrated in Chapters 6 and 7, PLASMiS probabilistically models SME microgrids both for average day scenarios and across hundreds of days with different parameters (e.g., weather types). Specifically, the tool runs Monte Carlo simulations on microgrid models, as discussed in Chapter 5, to generate numerical results and quantitatively evaluate rule-based operating and dispatch strategies.

Finally, the case studies in Chapter 7 show through simulations that sufficient load clipping reduces the incidence of power cuts in an islanded microgrid scenario. Case studies demonstrate the effects of changing storage discharge strategy, clipped load power limits, and the number of clipped loads. Results come from an islanded SME microgrid model based on data from central Rwanda, with parallels to microgrid scenarios across East Africa. The case studies provide insight into changing the clipped power limit for individual consumers, the number of consumer loads clipped, and the rationale for dispatching stored energy.

The results in Chapter 7 show that clipping customers is a DSM technique that can both reduce the incidence of power cuts and increase the levels of energy sold. The results also demonstrate that more clipping is not always better, but in fact an optimal level of load clipping exists depending on the grid operator's goals, e.g., maximizing renewable energy sold or minimizing the incidence and duration of power cuts. The example presented found that half of the option space for clipping decisions constituted over-clipping and did not serve the operator or customers optimally. Rather, these operating points unnecessarily clipped customers such that total energy sold was reduced and the time spent in power cut or clipping states was not reduced when compared to the optimal setting which allowed moderate clipping of half the house loads.

8.2 Future Work

The case studies in Chapter 7 demonstrate how load clipping can increase grid reliability and energy sold. In addition to lowering the incidence of power cuts, clipping and cutting individual loads can reduce the amount of fuel-burning generation required to operate the microgrid. This research is therefore a first step in determining the target number of homes in which to install smart meters and the pricing (tariffs plus unit and installation costs) that would improve

environmental sustainability as well as profitability. PLASMiS can model the number of loads in an existing system to project financial results of instrumenting specific loads with smart meters. In this way PLASMiS can de-risk plans to incorporate smart meters into legacy systems by providing established microgrid operators an evaluation tool [66], [58].

One area for future work is dynamic clipping levels, both in terms of changing clipped power limits and changing the number of clippable loads. Dynamic clipping would benefit microgrids by ensuring sufficient clipping and preventing the over-clipping discussed in Case Study 4. The precise level of clipping needed varies depending on unclipped load and stored energy, among other factors. The levels of nondispatchable supplies further affect the level of clipping needed, and these supply levels change based on the day's weather.

As discussed in Chapter 3, the choice of computing aggregate loads rather than each individual load improves computational efficiency and runtime in PLASMiS. This decision to track aggregate loads rather than individuals unfortunately prevents knowing or controlling individual load levels. Approximation is therefore required so long as this aggregation approach is kept. Using the methods of clipped aggregate estimation from Section 3.5, the instananeous level of clipping benefit (i.e., aggregate load reduction from clipping) could be chosen dynamically with a slightly modified EM model. This method assumes no results are needed regarding which loads (or how many) are clippable at a given time. Similarly, the exact clipping limit imposed on clipped loads is unknown in this method. Aggregate load reduction alone is prescribed, rather than individual load clipping limits or instantaneous state (clipped or unclipped).

A method which would allow dynamic changes to the number of clippable loads could come from a more sophisticated EM model with multiple discrete options for clippable and unclippable aggregate load curves. In pre-processing, a few pairings of clippable and unclippable aggregate loads could be computed for different breakdowns of the total aggregate load. This would allow the needed clippable and unclippable subsets to be combined pairwise depending on the number of clippable loads chosen at a given time by the EM.

Modeling a utility grid connection in modeled microgrids would extend the usefulness of PLASMiS beyond the scope of islanded microgrids alone. The simplest utility grid connection would sell power to the microgrid but not buy power generated in the microgrid. A one-way utility grid connection of this sort would be modeled as a supply similar to hydro. A more

general model of utility grid connection would allow power to flow both ways and would be modeled like battery storage. Constraints on power flowing in or out of a utility grid could be limited based on time of day (e.g., if the utility only sells power to the microgrid at low demand hours when its supply resources are typically below maximum output). Alternatively, the power demanded and/or sold from the utility grid could be generated randomly with time-of-day-dependent probability distributions either Markovian or independent in time. In this most generalized model of a utility grid connection, power curves would be generated with probabilistic models as discussed in Chapter 3. If the utility grid both buys and sells power, the resulting probability distributions could be sampled to produce positive or negative power values any given time step.

Regarding storage, battery scheduling can be optimized with plots of battery charging and discharging limits over the time required to charge and discharge. These plots (characterizing lead aid and lithium ion batteries, respectively) have been generated from industry specifications for future use with PLASMiS. The plots would prove useful in an EM that forecasts demand in advance or a controller that prioritizes complete charging or discharging at certain times of day. Depending on how long a full charge or discharge will take from the present SOC, the EM could schedule when to begin charging or discharging for a projected length of time.

Electricity pricing is important for incentivizing customers to change their demand patterns and for supporting the microgrid infrastructure financially. The tests presented in this dissertation, specifically case studies 3 and 4, show scenarios more energy can be sold by clipping than by leaving loads unclipped. Optimization with respect to pricing, and especially tiered pricing for customers with different clipping plans, is left for future work. To smooth the aggregate load curve and prevent rolling blackouts, electricity pricing can be tied to clipped power limits, enforced as needed by clipping DSM. Price incentivizes could lead consumers to accept lower limits at times of clipping, which could flatten the load curve and reduce the likelihood of power cuts.

Enhancing the tool with electricity pricing metrics requires tailoring for the specific objectives of a project owner (e.g., a microgrid operator) or stakeholders/shareholders (e.g., customers that collectively plan or run a microgrid). The utility function to optimize will differ depending on the chosen party of interest. The party of interest also affects the choice of dispatch, DSM, and

storage strategy. A microgrid operator, for example, will likely seek to maximize net income and protect the generation and storage assets, even if this means a higher incidence of clipping and cutting. A cooperative of customers purchasing power, on the other hand, will typically seek to improve quality of service and minimize the incidence of clipping and cutting.

Another area to enhance the tool is by incorporating certain real-world artifacts like loss of communication between smart meters and the EM. Communication loss could be simulated as a dynamic change in the number of clippable loads, where only loads in current communication with the EM are in fact clippable for a given time step. Simulations that vary the number of clippable loads could be constructed by computing and varying multiple pairwise combinations of clippable and unclippable loads, as described in the above discussion of dynamic clipping. This would allow the needed clippable and unclippable subsets to be combined pairwise depending on the number that have instantaneously lost communication with the EM, making those loads temporarily unclippable. Different combinations of clippable and unclippable loads could be generated probabilistically to account for levels of communication loss that vary stochastically throughout each day.

Finally, questions of equity and customer choice are vital to socially-conscious and environmentally sustainable microgrid development. For example, a model that includes customer choice could probabilistically model individual customers opting not to be clipped at certain times (i.e., temporarily becoming unclippable at their own discretion). Future work includes applying PLASMiS to address equity in energy access, reliable distribution, and affordable pricing. The tool can be used to develop metrics and incentives for social equity and sustainability in microgrid contexts.

Bibliography

[1] BYD P6C-36 Series-3BB PV module. *BYD Company Limited*, October 2013. http://www.byd.com/br/pv/. 52

[2] Power supply design for smart meters. *Digi-key Electronics*, October 2013. https://www.digikey.com/en/articles/techzone/2013/oct/power-supply-design-for-smart-meters. 7

[3] A designer's guide to lithium (Li-ion) battery charging. *Digi-key Electronics*, June 2016. https://www.digikey.com/en/articles/techzone/2016/sep/a-designer-guide-fast-lithium-ion-battery-charging. 37

[4] Pika Home Wind Turbine T701 Manual and Data Sheet. *Pika Energy*, 2016. www.pika-energy.com/pika-home-wind-turbine-t701, accessed Sept. 30, 2016. 33

[5] About us. *Meteoblue*, 2018. https://content.meteoblue.com/en/about-us. 48

[6] ASYV, Rwanda, 8.5 mw. *Scatec Solar*, 2018. https://www.scatecsolar.com/Portfolio/Rwanda/ASYV-Rwanda-8.5-MW. 52

[7] Climate Kigali. *Meteoblue*, 2018. https://www.meteoblue.com/en/weather/forecast/ modelclimate/kigali_rwanda_202061. 49

[8] GridLAB-D. June 2018. https://www.gridlabd.org/. 11, 12

[9] HOMER energy. March 2018. https://homerenergy.com. 10

[10] Microgrid definitions. *Microgrids at Berkeley Lab, Grid Integration Group, Energy Storage and Distributed Resources Division, Lawrence Berkeley National Laboratory*, 2018. https://building-microgrid.lbl.gov/microgrid-definitions. 1

[11] Products and services: power manager. *Duke Energy Corporation*, 2018. https://www.duke-energy.com/home/products/power%20manager?jur=NC01. 60

[12] Smart electricity meter market size, share & trends analysis report by end-use (residential, commercial, industrial), by region (North America, Europe, Asia Pacific, South America, MEA), and segment forecasts, 2018 - 2025. Industry 978-1-68038-074-3, Grand View Research, April 2018. 8

[13] Y. Arafat, L. B. Tjernberg, and S. Mangold. Feasibility study on low voltage dc systems using smart meter data. In *Proceedings of the 22nd International Conference and Exhibition on Electricity Distribution (CIRED)*, pages 1–4, June 2013. 7

[14] C. Barbulescu, G. Vuc, S. Kilyeni, D. Jigoria-Oprea, and O. Pop. Transmission planning – a probabilistic load flow perspective. *International Journal of Energy and Power Engineering*, 17:665–670, 2008. 10, 13

[15] L. Bauer and S. Matysik. AN Bonus 150/30 - 150,000 - wind turbine. 2018. https://en.wind-turbine-models.com/turbines/124-an-bonus-150-30. 52

[16] R. N. Bracewell. *The Fourier transform and its applications*. McGraw-Hill, New York, NY, 2000. 20

[17] P. Buchana and T. S. Ustun. The role of microgrids and renewable energy in addressing sub-Saharan Africa's current and future energy needs. *IEEE IREC*, March 2015. 10

[18] M. Buevich, D. Schnitzer, T. Escalada, A. Jacquiau-Chamski, and A. Rowe. Fine-grained remote monitoring, control and pre-paid electrical service in rural microgrids. *ACM/IEEE IPSN*, pages 1–11, April 2014. 1, 2, 6, 7, 8, 9, 31, 51

[19] M. Buevich, X. Zhang, O. Shih, D. Schnitzer, T. Escalada, A. Jacquiau-Chamski, J. Thacker, and A. Rowe. Short paper: Microgrid losses: When the whole is greater than the sum

of its parts. In *Proceedings of the 2nd ACM International Conference on Embedded Systems for Energy-Efficient Built Environments*, pages 95–98, Seoul, South Korea, November 2015. 10

[20] C.-F. Chuang, T.-R. Chen, and T.-C. Chen. Optimization of lead-acid battery charging for small uninterrupted power supply (ups). In *Proceedings of the National Science Council, Republic of China, Part A*, volume 25, pages 377–383, 2001. 53

[21] D. Deka, S. Backhaus, and M. Chertkov. Learning Topology of the Power Distribution Grid with and without Missing Data. *ArXiv e-prints*, March 2016. 9

[22] E.O. Diemuodeke, E.O. Agbalagba, and M.I. Okorho. Building integrated hybrid pv-battery-diesel generator energy system for oil producing communities in niger-delta region of nigeria. *International Journal of Renewable Energy Research*, 4(2):286–293. 52

[23] S. Finger. Electric power system production costing and reliability analysis. *MIT Energy Laboratory MIT-EL-79-006*, February 1979. 50

[24] P.A. Gagniuc. *Markov chains: From Theory to Implementation and Experimentation*. John Wiley and Sons, 2017. 15, 19

[25] A. González-García, P. Ciller, C. Drouin, R. Stoner, and I. P. Arriaga. Review assessment of current electrification programs prepared by REG / EDCL and confirmation on institutional, technical and financial aspects. Technical report, Tata Power-DDL and MIT–Comillas UEA Lab and EcoSecure Holding, Madrid, Spain, 2018. 2

[26] R.L. Graham and P. Hell. On the history of the minimum spanning tree. *Annals of the History of Computing*, 7(1):43–57, January 1985. 10

[27] G.R. Grimmett and D.R. Stirzaker. *Probability and random processes*, volume 80. Oxford university press, 2001. 13, 15, 18

[28] E. Hittinger, T. Wiley, J. Kluza, and J. Whitacre. Evaluating the value of batteries in microgrid electricity systems using an improved energy systems model. *Energy Conversion and Management*, 89:458–472, May 2014. 2

[29] G. Hug, M. Zima, and A. Ulbig. Power system dynamics, control and operation. Lecture notes for course 227-0528-00L, ETH Zurich, Zurich, Switzerland, February 2016. pp. 105–119. 30

[30] World Bank Institute. Rwanda: energy learning overview. 2016. wbi.worldbank.org/energy/case-studies/rwanda. 51

[31] B. Jabeck. The impact of generator set underloading, October 2014. 52

[32] R. Jamil et al. Theoretical studies of automatic generation control technology. *International Journal of Innovation and Applied Studies*, 4(4):636–642, December 2013. 38

[33] H. Keshan, J. Thornburg, and T. S. Ustun. Comparison of lead-acid and lithium ion batteries for stationary storage in off-grid energy systems. In *Proceedings of the IET International Conference on Clean Energy and Technology*, November 2016. 31, 36, 37

[34] C. D. Korkas et al. A supervisory approach to microgrid demand response and climate control. In *Proceedings of the Mediterranean Conference on Control and Automation*, pages 1140–1145, June 2016. 33

[35] Dirk P. Kroese, Tim Brereton, Thomas Taimre, and Zdravko I. Botev. Why the Monte Carlo method is so important today. *Wiley Interdisciplinary Reviews: Computational Statistics*, 6(6):386–392. 16

[36] F. Kupzog, T. Zia, and A. A. Zaidi. Automatic electric load identification in self-configuring microgrids. In *Proceedings of the IEEE AFRICON*, Nairobi, Kenya, January 2009. IEEE PES. 7

[37] T. Lambert, P. Gilman, and P. Lilienthal. *Micropower system modeling with HOMER*. John Wiley and Sons, Inc., 2006. 11

[38] M. Lee, G. C. Shaw, and V. Modi. Battery storage: Comparing shared to individually owned storage given rural demand profiles of a cluster of customers. In *Proceedings of the IEEE Global Humanitarian Technology Conference*, San Jose, CA, USA, October 2014. 53

[39] X. Li and O. A. Omitaomu. Optimal solar pv arrays integration for distributed generation. In *Proceedings of the Institute of Industrial Engineers Annual Conference*, pages 1–9, Orlando, FL, USA, 2012. 9

[40] W. N. Macêdo and R. Zilles. Operational results of grid-connected photovoltaic system with different inverter's sizing factors (isf). *Progress in Photovoltaics: Research and Applications*, 15(4):337–352, 2006. 9

[41] P. Mahat et al. A micro-grid battery storage management. In *Proceedings of the IEEE Power and Energy Society General Meeting*, July 2013. 36

[42] E. Maniraguha. The utilization of wind power in Rwanda. master's thesis, KTH School of Industrial Engineering and Management, Stockholm, Sweden, 2013. 52

[43] M.-G. D. Manual. Energy sector management assistance programme (ESMAP). Technical Report 007, UNDP/World Bank, April 2000. 8

[44] A. G. Manur. Microgrid energy management system. Master's thesis, University of Wisconsin-Madison, Madison, WI 53706, December 2015. 7

[45] J. McCalley. AGC 1. Lecture notes for course EE 457, Iowa State University, Ames, IA, USA, 2016. pg. 1. 38

[46] J. Mugabo. Mobisol solar system to help Burundian refugees. *The New Times*, October 2015. 51

[47] A. Narayan. *A Framework for Microgrid Planning Using Multidisciplinary Design Optimization*. PhD thesis, University of Waterloo, Waterloo, ON, CA, 2015. 13

[48] A. Niinisto. Simulation of the management of a micro grid with wind, solar and gas generators. master's thesis, Aalto University School of Science and Technology, Helsinki, Finland, 2009. 8

[49] O. A. Omitaomu and B. L. Bhaduri. Prediction of solar radiation on building rooftops: A data-mining approach. *62nd IIE Annual Conference and Expo 2012*, January 2012. 9

[50] H. Oueslati, S. Ben Mabrouk, A. Ben Mabrouk, F. Massaro, G. Zizzo, L. Dusonchet, and S. Favuzza. Feasibility analysis and study of a grid-connected hybrid electric system: application in the building sector. In *Proceedings of the IEEE 16th International Conference on Environment and Electrical Engineering*, Florence, Italy, June 2016. 10

[51] T. G. Quetchenbach et al. The GridShare solution: a smart grid approach to improve service provision on a renewable energy mini-grid in Bhutan. *Environmental Research Letters*, 8(1):014018, 2013. 2, 6, 7, 9

[52] N. S. Rastogi. You charged me all night long. *Slate*, March 2012. https://slate.com/technology/2012/03/is-charging-your-cell-phone-overnight-a-major-waste-of-energy.html. 51

[53] A. Rowe. Rural microgrids. *Wireless, Sensing, and Embedded Systems (WiSE) Lab, Carnegie Mellon University*, July 2014. http://wise.ece.cmu.edu/redmine/projects/microgrid/wiki. 7

[54] B. Sergi, M. Babcock, N.J. Williams, J. Thornburg, A. Loew, and R.E. Ciez. Institutional influence on power sector investments: A case study of on- and off-grid energy in Kenya and Tanzania. *Energy Research and Social Science*, 41:59–70, 2018. cited By 4. 2

[55] M. Smith. U.S. Department of Energy's research and development activities on microgrid technologies. In *Proceedings of the 2010 Vancouver Symposium on Microgrids*, July 2010. 1

[56] P. Sreedharan et al. Assessing the business case for rural solar microgrids in india: a case study approach. Technical report, U.S. Trade and Development Agency, October 2014. 7

[57] D. D. Tewari and T. Shah. An assessment of South African prepaid electricity experiment, lessons learned, and their policy implications for developing countries. *Energy Policy*, 31(9):911 – 927, 2003. 8

[58] J. Thornburg, G. Hug, T. S. Ustun, A. Rowe, and B. Krogh. Incorporating smart-grid operating strategies into off-grid electrification planning. In *Proceedings of the SIAM Conference on Control and Its Applications*, Paris, France, July 2015. 2, 6, 13, 30, 45, 60, 71

[59] J. Thornburg and B. Krogh. Simulating energy management strategies for microgrids with smart meter demand management. In *Proceedings of the IEEE Power and Energy Society PowerAfrica*, Accra, Ghana, June 2017. 2, 6, 12, 13, 30, 33, 37, 45, 47, 70

[60] J. Thornburg, B. Krogh, and T. S. Ustun. Stochastic simulator for smart microgrid planning. In *Proceedings of the ACM Symposium on Computing and Development (DEV)*, Nairobi, Kenya, November 2016. 2, 6

[61] J. Thornburg, T. S. Ustun, and B. Krogh. Smart microgrid operation simulator for management and electrification planning. In *Proceedings of the IEEE Power and Energy Society PowerAfrica*, Livingstone, Zambia, June 2016. 2, 6, 12, 13, 30, 45

[62] J. Tobe. Managing battery charging using diversion loads. *Home Power Inc.*, (166), March 2015. https://www.homepower.com/articles/wind-power/design-installation/managing-battery-charging-using-diversion-loads/page/0/2. 36

[63] F. Tuffner. GridLAB-D – dynamic simulation capabilities. *Pacific Northwest National Laboratory*, January 2018. Presented at WECC Model Validation Working Group. 11

[64] P. Tumwebaze. MININFRA: wind energy in Rwanda – in which direction will the wind blow? *The New Times*, May 2008. 52

[65] D. Turcotte, M. M. D. Ross, and F. Sheriff. Photovoltaic hybrid system sizing and simulation tools: Status and needs. *PV Horizon : Workshop on Photovoltaic Hybrid Systems*, September 2001. 9

[66] T. S. Ustun, J. Thornburg, and B. Krogh. Smart pricing implementation/simulator with ICT infrastructure. In *Proceedings of the Africa-EU Symposium on Renewable Energy Research and Innovation*, Tlemcen, Algeria, March 2016. 7, 9, 71

[67] V. Vanitha et al. Control of microgrid with enhancement of wind power evacuation. *Wind Engineering*, 39(5):529–532, 2015. 29, 34, 44

[68] K. Vatanparvar. Design space exploration and energy management in residential microgrids. Master's thesis, University of California, Irvine, 2015. 12

[69] G. Venkataramanan and C. Marnay. A larger role for microgrids. *IEEE Power and Energy Magazine*, 6(3):78–82, May 2008. 2

[70] L. Wan, W. Lou, E. Abner, and R. J. Kryscio. A comparison of time-homogeneous Markov chain and Markov process multi-state models. *Communications in Statistics: Case Studies, Data Analysis and Applications*, 2:92–100, 10 2016. 15

[71] T. Wei et al. Co-scheduling of HVAC control, EV charging and battery usage for building energy efficiency. In *Proceedings of the IEEE/ACM International Conference on CAD*, pages 191–196, November 2014. 8

[72] M Welsch et al. Smart and just grids for sub-Saharan Africa: exploring options. *Renewable and Sustainable Energy Reviews*, 20:336–352, 2013. 7

[73] N. J. Williams. *Microgrid Utilities for Rural Electrification in East Africa: Challenges and Opportunities*. PhD thesis, Carnegie Mellon University, Pittsburgh, PA, May 2017. 11, 12, 13

[74] N. J. Williams, P. Jaramillo, B. Cornell, I. Lyons-Galante, and E. Wynn. Load characteristics of East African microgrids. In *Proceedings of the IEEE Power and Energy Society PowerAfrica*, pages 236–241, Accra, Ghana, June 2017. 10

[75] N. J. Williams, P. Jaramillo, and J. Taneja. PV-array sizing in hybrid diesel/PV/battery microgrids under uncertainty. In *Proceedings of the IEEE Power and Energy Society PowerAfrica*, pages 189–193, Livingstone, Zambia, June 2016. 11, 13

[76] N. J. Williams, P. Jaramillo, J. Taneja, and T. S. Ustun. Enabling private sector investment in microgrid-based rural electrification in developing countries: A review. *Renewable and Sustainable Energy Reviews*, 52:1268 – 1281, 2015. 2

[77] E. Wood. Eaton adds name to growing list offering microgrid controllers. *Microgrid Knowledge*, December 2015. https://microgridknowledge.com/eaton-adds-name-to-growing-list-offering-microgrid-controllers/. xii, 7, 8

[78] S. Zameer. Securing the smart energy revolution in Africa. *Ventures Africa*, October 2018. http://venturesafrica.com/apostories/securing-the-smart-energy-revolution-in-africa/. 7, 8

[79] E. Zare and M. Shahabi. Microgrid restoration after major faults in main grid with automatic and constant time switching. *International Journal of Intelligent Systems and Applications*, 5(10):50–58, 2013. 36

[80] K. Zipp. 4 ways to maximize a microgrid. *Solar Power World*, January 2016. https://www.solarpowerworldonline.com/2016/01/24443/. 53

[81] A. Zisserman. 2D Fourier transforms and applications. Lecture notes for B14 Image Analysis, Oxford University, September 2014. 20